uOttawa

L'Université canadienne
Canada's university

FACULTÉ DES ÉTUDES SUPÉRIEURES ET POSTOCTORALES

uOttawa

L'Université canadienne
Canada's university

FACULTY OF GRADUATE AND POSDOCTORAL STUDIES

Dave McPhee

AUTEUR DE LA THÈSE / AUTHOR OF THESIS

M.A.Sc. (Electrical Engineering)

GRADE / DEGREE

School of Information Technology and Engineering

FACULTÉ, ÉCOLE, DÉPARTEMENT / FACULTY, SCHOOL, DEPARTMENT

Efficient Method for the Computation of Parasitic Coupling in Microwave Integrated Circuits

TITRE DE LA THÈSE / TITLE OF THESIS

M. Yagoub

DIRECTEUR (DIRECTRICE) DE LA THÈSE / THESIS SUPERVISOR

CO-DIRECTEUR (CO-DIRECTRICE) DE LA THÈSE / THESIS CO-SUPERVISOR

EXAMINATEURS (EXAMINATRICES) DE LA THÈSE / THESIS EXAMINERS

D. McNarmara

L. Roy

Gary W. Slater

LE DOYEN DE LA FACULTÉ DES ÉTUDES SUPÉRIEURES ET POSTDOCTORALES /
DEAN OF THE FACULTY OF GRADUATE AND POSTDOCORAL STUDIES

EFFICIENT METHOD FOR THE COMPUTATION OF PARASITIC COUPLING IN MICROWAVE INTEGRATED CIRCUITS

By

Dave McPhee, B. Eng.,

A thesis submitted in partial fulfillment of the requirements for the degree of

Master of Applied Science

University of Ottawa

2005

Your file Votre référence
ISBN: 0-494-11350-2
Our file Notre référence
ISBN: 0-494-11350-2

ABSTRACT

Higher integration and smaller layout size, two major trends in today's industry, lead to more prominent parasitic electromagnetic coupling effects in high-frequency communication systems. Using network theory concepts and de-embedding techniques, this thesis presents a fast and efficient method to model such coupling in microwave integrated circuits, making the design more reliable. The efficiency of the new technique is demonstrated through examples of circuit simulations and circuit optimization.

ACKNOWLEDGMENTS

This thesis is dedicated to my wife, Eun Woo Kim-McPhee. Through any achievement or hardship I faced, my wife stood steadfastly and resolutely behind me offering love, encouragement, support and lunch.

This thesis would not have been possible without the thoughtful and timely help of Dr Yagoub whom I consider more than just a mentor but a friend also. Dr Yagoub provided the direction and guidance necessary for this report to be completed successfully.

I would also like to thank Prasun Sharma for his many hours of consultation and reviewing. His help was invaluable and he spent of his own time expecting nothing in return. Thanks Prasun.

TABLE OF CONTENTS

CHAPTER I - INTRODUCTION

CHAPTER II – EM COUPLING

CHAPTER III - MODELING USING S-PARAMETER TECHNIQUES AND ELECTROMAGNETIC OPTIMIZATION

CHAPTER IV – RESULTS

CHAPTER V - CONCLUSION

APPENDIX

LIST OF FIGURES

LIST OF TABLES

CHAPTER I

INTRODUCTION

1.1 Motivation

The future of communications will be dominated by ever-increasing signal through rates and bandwidth requirements. Currently, there is tremendous opportunity to take advantage of circuits operating at higher frequencies. For instance, circuits designed at millimeter wave frequencies can have significant advantages over circuits designed at radio frequencies in terms of bandwidth and cost. As recently as 1996, the 59-64 GHz band has been opened by the U.S. Federal Communications Commission (FCC) for non-government use [FCC]. This spectral band is of major interest since a large amount of bandwidth has been allocated for wireless communications. Such a large bandwidth has the distinguishing ability to carry large numbers of broadband data simultaneously [Tuyl96]. As such, 60 GHz band wireless systems will contribute part of a fourth

generation (4G) telecommunication system [Smul02]. Possible applications of 60 GHz systems include 60 GHz Wireless Local Area Networks (WLAN) [Smul02] [Gord04] [Siam03], Wireless Ethernet [Ohat03] and Automotive Radar [Gord04] [Tuyl96].

Furthering this trend has been a host of new enabling technologies which have increased the performance and speed of Monolithic Microwave Integrated Circuits (MMICs) or reducing the cost. Gallium Arsenide (GaAs) circuits initially led the way in MMIC circuit design. Cutoff Frequencies (f_T) for transistors designed using GaAs process technology has been reported to be as high as high as 170 GHz [Iwam03].

GaAs process technology is still relatively expensive due to extra process steps required to integrate with CMOS logic. Recently Silicon Germanium (SiGe) process technology has been introduced which addresses this problem and is a leading technology towards the utilization of the 60GHz band. SiGe retains many of the benefits of GaAs in terms of high f_T and gain, while introducing compatibility with CMOS processing [Laur03]. This provides SiGe with a cost benefit over other processes since CMOS is the industry cost leader. Furthermore, industry is leading toward higher integration where large designs are integrated onto a single die, which is referred to as System on a Chip (SoC). Higher integration yields benefits in performance and cost but in order to achieve these designs the die size must remain small enough to maintain high yields. To summarize, SiGe can be an enabling technology to cost leading designs that incorporate the SoC design approach, but it is essential that MMIC design must remain as small as possible.

Design of densely packed small components is a challenging research area. Matching and Filtering at Millimeter Wave frequencies tend to be in the form of distributed elements which consume large die area. While knowing that die area is crucial for yield and SoC design, new research has explored the use of lumped elements for MMICs instead of distributed elements. It was shown that a lumped element based Low Noise Amplifier (LNA) [Gord04] can be fabricated which occupies 5 times less area than a comparable distributed element based LNA [Reyn04] while having similar performance at over 50GHz. Through the use of lumped elements, large saving in terms of die area can be achieved at the cost of slightly degraded results and higher power consumption.

Lumped elements at high frequencies are also extensively used in Multi Chip Modules (MCMs) [Shar04]. MCM mount multiple chips inside a single package, and can incorporate many lumped elements. Therefore, MCM can reduce the overall footprint of a circuit on the motherboard over single chip approaches. In this application, lumped elements are a very attractive alternative over distributed elements because they can consume less area which is at a premium inside the MCM.

Even though the use of lumped elements at high frequencies are extremely important to emerging technologies like SoCs and MCMs, design using lumped elements at high frequencies is subject to high parasitics and electromagnetic (EM) coupling. Coupling is a general term used to describe EM field interactions between two structures. Distributed and mutual coupling, which result from EM field interactions in the network, exert a significant effect on integrated circuits [Yago04]. This parasitic effect can

become more of a concern in SoCs and MCMs as packing densities of components are increased and frequencies are pushed even higher [Dunn93]. For instance in a densely packed MIC amplifier using lumped elements, coupling can cause the centre frequency and magnitude to shift significantly from the expected results depending on the layout and frequency of operation. Although such unintended coupling between components plays an important role in the circuit performance, this quantity is very complex to evaluate. Existing lumped- or physical/geometrical-based models do not adequately include all electromagnetic (EM) effects. Alternatively, although EM-based models are accurate, they cannot be easily implemented in a circuit simulator and are time consuming to generate. Until recently, it has been practice to effectively ignore EM coupling in lumped elements since the effect is less prominent at the lower side of the microwave spectrum. However, with the increase of operating frequencies up to the millimeter range, new designs using lumped elements instead of distributed elements have been presented at frequencies higher than 40 GHz where EM effects can be significant [Yago04]. These include, for instance, a 50GHz Mixer by Dickson [Dick05], and a 52 GHz LNA by Gordon [Gord04].

In the recent years, several techniques in bringing the coupling phenomenon forward into the circuit design space have been investigated [Yago04] [Gold91] [Ding01] [Baud97]. The coupling phenomenon exists at such a high frequency that full wave EM simulation tools are required which are primarily based on the solution of Maxwell's equations to quantify the EM field in a structure. Such advanced full wave EM simulation tools include Sonnet *em* [Sonnet], and Ansoft *HFSS* [HFSS]. These tools

have demonstrated their efficiency in terms of accuracy, but still require huge computation time and memory space. This aspect is crucial when modern Computer Aided Design (CAD) tools lead to massive and highly repetitive computational tasks during simulation, optimization and statistical analysis. As such, development of fast and full EM representations with high-order coupling is crucial for modern circuit design. Furthermore, existing lumped element EM-based models suffer on an important lack at the circuit level. In fact, even if such device models are accurate, they are developed in a perfect shielded environment, i.e., excluding any external effects such as coupling with neighboring components.

This thesis introduces a fast and accurate technique that efficiently integrates interactions between circuit elements in microwave circuit simulators. Using simple network theory concepts and de-embedding techniques [Chen01], this original approach allows efficient evaluation of parasitic coupling during design. The aim is to insert coupling between lumped elements as an additional and separate component in any type of network. Using these so called coupling models, system-wide EM simulations can be broken into component level pieces. Breaking down an overall simulation in this way can aid in system wide optimization and design since these models can be relatively easily exported to commercial circuit simulators.

1.2 Contributions Overview

1. The first contribution was a new method for modeling electromagnetic coupling. Coupling in series networks, parallel networks and finally arbitrarily connected networks were successfully modeled as a separate sub-network component. *T*-parameters were used for the series network formulation, while *Y*-parameters were used for the parallel network formulation. The Connection Scattering Matrix representation was employed for any other type of network including multi-port components.
2. The second contribution was to use the extracted coupling models in a circuit simulator for the first time. This combines the advantages of the speed of a circuit simulator with the accuracy of an EM based simulator including coupling. The coupling models are applied to the practical application of discrete optimization.

1.3 Thesis Overview

Chapter 2 begins by introducing the effect of coupling. General characteristics about coupling are presented. Background information is provided in chapter 2 for the EM tools used throughout this thesis, i.e., Sonnet *em* and Ansoft *HFSS*. In Chapter 3, we developed our method for coupling modeling in all circuit configurations namely series, parallel and arbitrary networks. Chapter 3 concludes by demonstrating how to apply the coupling models to an optimization. Chapter 4 discusses the results and Chapter 5 concludes the thesis with recommendations for future work.

1.4 Publications

In Journals:

- D. McPhee, M.C.E. Yagoub, "A generic procedure for exact high frequency device characterization using post-processing data," accepted for publication in the *Int. J. of Pure and Applied Mathematics.*
- D. McPhee, M.C.E. Yagoub, "Novel Approach for Efficient Electromagnetic Coupling Computation in RF/Microwave Integrated Circuits," accepted for publication in *WSEAS Trans. On Circuits.*

In Refereed Conferences:

- D. McPhee, M.C.E. Yagoub, "Efficient method for the computation of electromagnetic coupling in microwave integrated circuits," *2nd IASTED Int. Conf. on Antennas, Radar, and Wave Propagation* (ARP 2005), Banff, AB, July 19-21, 2005.
- D. McPhee, P. Sharma, M.C.E. Yagoub, "Characterization of higher-order electromagnetic coupling effects in RF/microwave circuits," *IEEE Int. Conf. on Communication, Computer and Power* (ICCCP'05), Feb. 14-16, 2005, Muscat, Oman.
- D. McPhee, M.C.E. Yagoub, "Efficient modeling of distributed electromagnetic coupling in RF/microwave integrated circuits," *4th Int. Conf. on Electronics, Signal Processing and Control* (ESPOCO 2005), Rio de Janeiro, Brazil, April 25-27, 2005.

1.5 References

[Baud97] H. Baudrand, "Electromagnetic study of coupling between active and passive circuits," *Int. Microwave and Optoelectronics Conf.*, 1997, 143-152.

[Chen01] C. Chen & M. Deen, "A general noise and sparameter deembedding procedure for on-wafer high-frequency noise measurements of MOSFETs," *IEEE Trans. On Microwave Theory Tech.*, 2001, 1004-1005.

[Dick05] T.Dickson, M.LaCroix, S.Boret, D.Gloria, R.Beerkens, S.Voinigescu, "30-100-GHz Inductors and Transformers for Millimeter-Wave (Bi)CMOS Integrated Circuits," *IEEE Trans. On Microwave Theory and Tech.*, 2005, 123-133.

[Ding01] X. Ding, B. Chattaraj, M.C.E. Yagoub, V.K. Devabhaktuni, & Q.J. Zhang, "EM based statistical design of microwave circuits using neural models," *Int. Symp. on Microwave and Optical Technology*, Montreal, Canada, 2001, 421-426.

[Dunn93] J.M. Dunn, L.C. Howard, & K. Larson, "An efficient algorithm for the calculation of parasitic coupling between lines in MIC's", *IEEE Trans On. Microwave Theory Tech*, 1993, 1287-1293.

[FCC] Federal Communications Commission amendment FCC 95-499, adopted and released Dec. 15, 1995.

[Gold91] M. Goldfarb & A. Platzker, "The effects of electromagnetic coupling on MMIC design," *Microwave & Millimeter Wave CAE*, 1991, 38-47.

[Gord04] M. Gordon and S. Voinigescu, "An Inductor-Based 52-GHz 0.18 um SiGe HBT Cascode LNA with 22 dB Gain," *Proceeding of the 30th European Solid-State Circuits Conference*, ESSCIRC 2004, 287 – 290.

[HFSS] Ansoft-HFSS v.8.0, Ansoft Corp., Pittsburg, PA.

[Iwam03] M. Iwamoto, D. Root, J. Scott, A. Cognata, P. Asbeck, B. Hughes, D. D'Avanzo, "Large-Signal HBT Model with Improved Collector Transit Time Formulation for GaAs and InP Technologies," *IEEE Trans. On Microwave Theory and Tech.*, 2003, 635 – 638.

[Laur03] M. Laurens, B. Martinet, O. Kermarrec, Y. Campidelli, F. Deleglise, D. Dutartre, G. Troillard, D. Gloria, J. Bonnouvrier, R. Beerkens, V. Rousset, F. Levard, A. Chantre, A. Monroy, "A 150GHz fT/fmax 0.13um SiGe:C BiCMOS technology," *Proceedings of the Bipolar/BiCMOS Circuits and Technology Meeting*, 2003, 199 – 202.

[Ohat03] K. Ohata, K. Maruhashi, M. Ito, S. Kishimoto, K. Ikuina, T. Hashiguchi, K. Ikeda, N. Takahashi, "1.25 Gbps wireless Gigabit ethernet link at 60 GHz-band," *2003 IEEE Radio Frequency Integrated Circuits (RFIC) Symposium*, 2003, 509 - 512.

[Reyn04] S. Reynolds, B. Floyd, U. Pfeiffer, T. Zwick, "60GHz Transciever Circuits in SiGe Bipolar Technology," *IEEE Solid-State Circuits Conference*, ISSCC 2004, 2004, 442 – 538.

[Shar04] P. Sharma, F. Mohammadi, M.C.E. Yagoub, "Neural Design and Optimization of RF/Microwave EM-based MultiChip Modules," *2004 RF and Microwave Conference*, 2004, Subang Malaysia.

[Siam03] A. Siamarou, "Broadband wireless local-area networks at millimetre waves around 60 GHz," *IEEE Antennas and Propagation Magazine*, 2003, 177 – 181.

[Sonnet] Sonnet 9.52, Sonnet Software Inc., Liverpool, NY.

[Smul02] P. Smulders, "Exploiting the 60GHz Band for Local Wireless Multimedia Access: Prospects and Future Directions," *IEEE Communications Magazine*, 2002, 140-147.

[Tuyl96] R. Tuyl, "Unlicensed Millimeter Wave Communications, A New Opportunity for MMIC Technology at 60 GHz," *18th Annual Gallium Arsenide Integrated Circuit (GaAs IC) Symposium*, 1996, 3 – 5.

[Yago04] M.C.E. Yagoub, P. Sharma, "Characterization of EM effects in RF/microwave integrated circuits," *34th European Microwave Conf.*, 2004, Amsterdam, Netherlands, 221-224.

CHAPTER II

EM COUPLING

EM Coupling can be defined as electric/magnetic field interaction between two structures. In passive circuits, coupling takes the form as either mutual coupling or distributed coupling. Mutual coupling refers to the EM field interaction between two distinct components such as between a resistor and a capacitor or between antenna elements [Ozde03]. On the other hand, distributed coupling is EM field interactions involving distributed elements. In many cases EM coupling can be a desirable behavior and is in use in many distributed filters and couplers. This thesis focuses on parasitic coupling present in many high frequency lumped circuit designs. Both mutual and distributed coupling are considered in this thesis.

As shown in figure 2-1, EM coupling can be present between a component and an interconnect (distributed coupling) as well as between tightly packed components (mutual coupling).

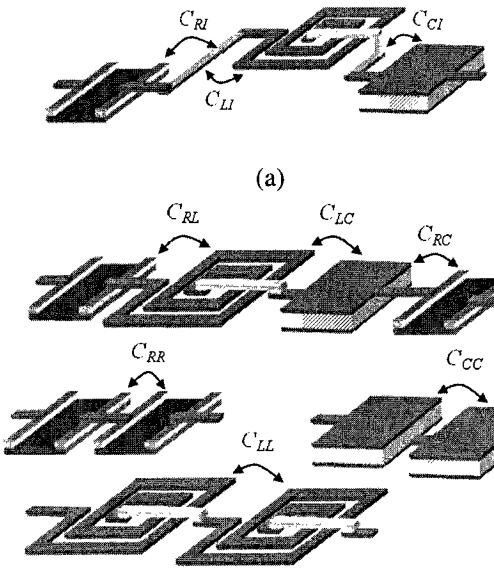

Figure 2-1. EM Couplings: (a) between Interconnect and Component, (b) Between Components. Subscripts *R*, *L*, *C* and *I* Refer to Resistors, Inductors, Capacitors, and Interconnects Respectively.

2.1 Coupling Background

At very high frequencies, lumped component models for passives do not include coupling effects. Thus said, a designer who models a high frequency circuit using simple lumped components will not obtain accurate results from simulation [Yago04]. The only recourse is to utilize a complicated fullwave electromagnetic simulation tool such as Sonnet *em* [Sonnet] or Ansoft *HFSS* [Ansoft]. The drawback to using such tools is the increased simulation complexity and resulting computation time needed to perform simulations.

Currently there is a wide variety of research focused on improving the speed and accuracy of high frequency simulation. Techniques have been presented on how to maximize use of

fast circuit simulators while maintaining the accuracy of electromagnetic simulators [Band94] [Rizz04]. Various methods have extended this work, including automatic data generation [Deva03] [Deva01], modeling using neural networks [Rizz04] [Zhan03] [Cho99] [Ding04], and optimization [Band93] [Xu03].

Coupling research has mostly been brought forward from the antenna/microwave community. This includes coupling in transmission lines [Lail02], interconnects [Zhao98], through apertures [Cast02]], in the PCB [Abdu02] [Abdu01] and mutual coupling in antenna arrays [Ozde03] to name a few.

Recently there has been activity in bringing this coupling research forward into the circuit design space. Erdin in 2000 presented his research on the analysis of coupling [Erdi00] using a full-wave simulator for the transmission lines as well as a circuit simulator. However, this method would be used for simulation purposes only (no prediction). The use of Neural Networks (NN) for modeling EM-based high frequency lumped components was explored by Ding [Ding04]. Using these NN models, a fast optimization of an amplifier was carried out. Although the individual lumped components were modeled accurately, mutual and distributed coupling were ignored, since each component was considered independently of the others. It has been demonstrated [Yago04] that coupling in circuit design introduces a non-negligible effect at higher frequencies in lumped components.

This paper is a continuation of the research in this field. Whereas [Yago04] demonstrated that coupling introduces a major effect at higher frequencies, this paper will attempt to model

this effect either by manipulating S-parameters, T-parameters or the Connection Scattering Matrix representation [Gupt81] of the circuit. While it is very true that integrated circuit geometry is arbitrary and will change with every different design, this research focuses on lumped components while assuming the fewest dimensions of design flexibility.

To obtain a qualitative understanding of electromagnetic coupling, a simple Resistor – Capacitor circuit is considered. The goal of this example is to demonstrate the effect of coupling between lumped components at different frequencies and at different interconnect lengths in both a series circuit and a parallel circuit. From this basic example, general conclusions can be made regarding coupling.

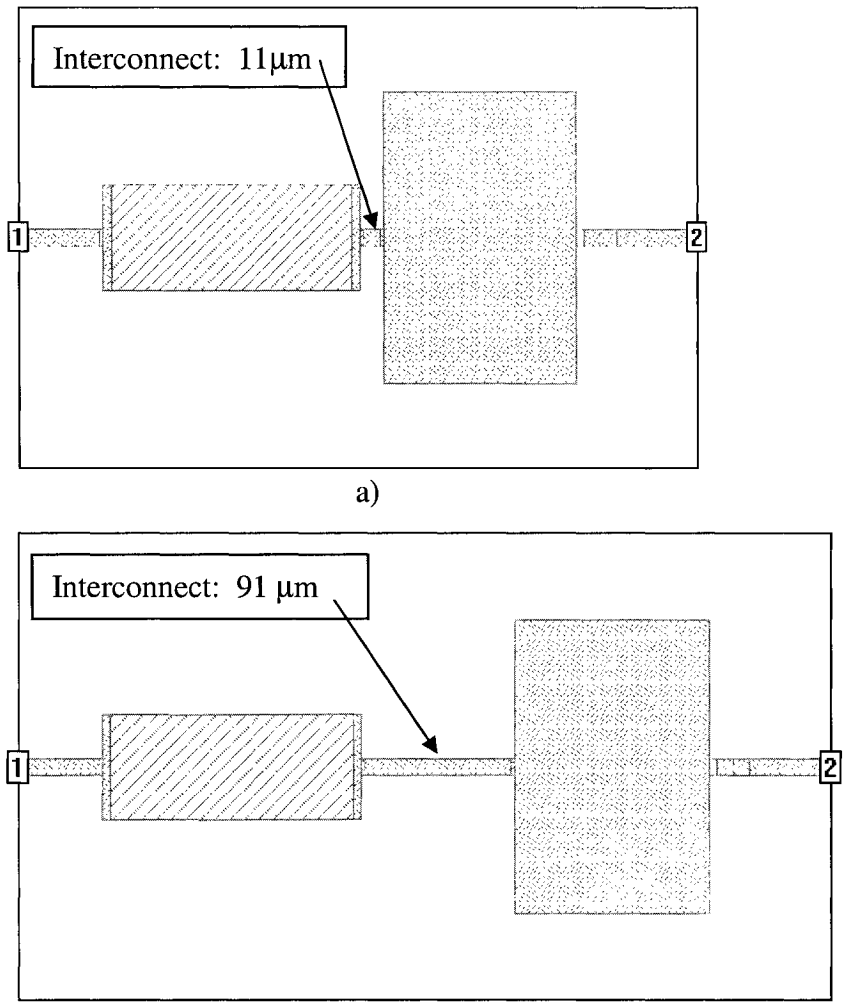

Figure 2-2. RC circuit considered in series coupling example. Examples shown are for (a) interconnect length of 11μm, (b) interconnect length of 91μm.

The circuit was with a 120μm thick GaAs Substrate (ε_r = 12.9). The 150μm x 65μm resistor was made from 40 Ohms/ Square resistive material. The measured resistance is 90 ohms. The capacitor has dimensions of 120μm x 180μm. The distance between the plates is 1μm and the measured capacitance is approximately 0.27pF.

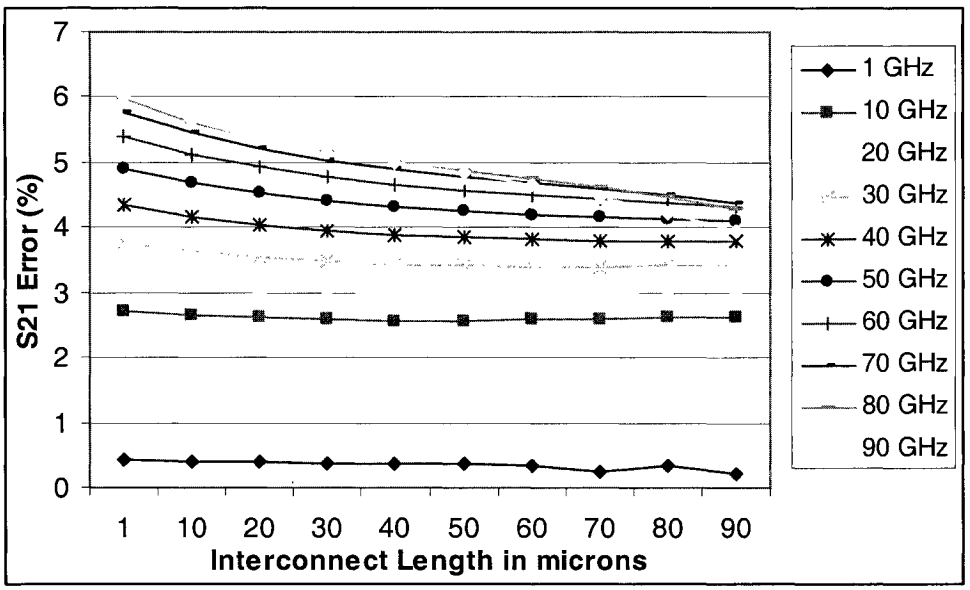

Figure 2-3. Coupling induced errors as a function of Interconnect length in microns and frequency for the series RC circuit.

Let $[S_i]$ be the computed equivalent scattering matrix of the two RC elements in cascade (using the individual $[S_R]$ and $[S_c]$ matrices of R and C respectively, i.e., without mutual or distributed coupling), and let $[S_w]$ the simulated matrix of the whole structure (i.e., including coupling). We defined a percentage error as the difference between the related S_{21} parameters:

$$\text{Error } \% = \left| \frac{|S_{21w}| - |S_{21i}|}{|S_{21i}|} \right| * 100 \qquad (2.1)$$

In figure 2-3, ten series RC circuit configurations with interconnect lengths ranging from 1 to 91μm were simulated from 1 to 90 GHz. It has been found that the effects of coupling in lumped components depend on several factors. Chief among these factors are component type, geometry and frequency. Higher frequencies exhibit much higher effects due to

coupling as can be seen in the series RC circuit simulation. At lower frequencies, the coupling has almost no effect irrespective of the distance between the components. The other factor that influences the effect of coupling was the interconnect length, although the coupling at higher interconnect lengths could also be due to increased distributed coupling between the component (R or C) and the interconnect. This was very evident for the coupling at 10-30 GHz.

A parallel implementation was considered next. This parallel RC circuit uses exactly the same components as the series circuit shown in figure 2-2. In this case, the distance between the two components was varied as shown in figure 2-4.

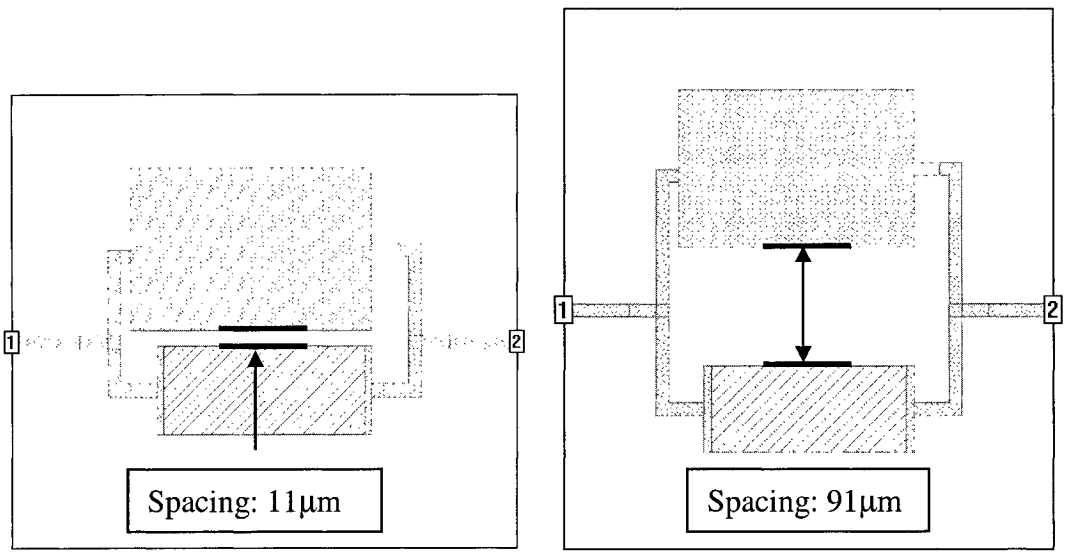

a) b)

Figure 2-4. RC circuit considered for parallel coupling example. Examples shown are for spacing of (a) 11μm and (b) 91μm.

The results for the parallel structure are shown in figure 2-5. From this result we can note that the parallel structure exhibits higher effects of coupling than the series structure using identical elements. This phenomenon could result from several possible factors. The largest contributing factor to this is that the relative area available for the components to couple is higher in the parallel structure. Similar to the series structure, the parallel structure's coupling characteristics have high dependence on both frequency and distance between components.

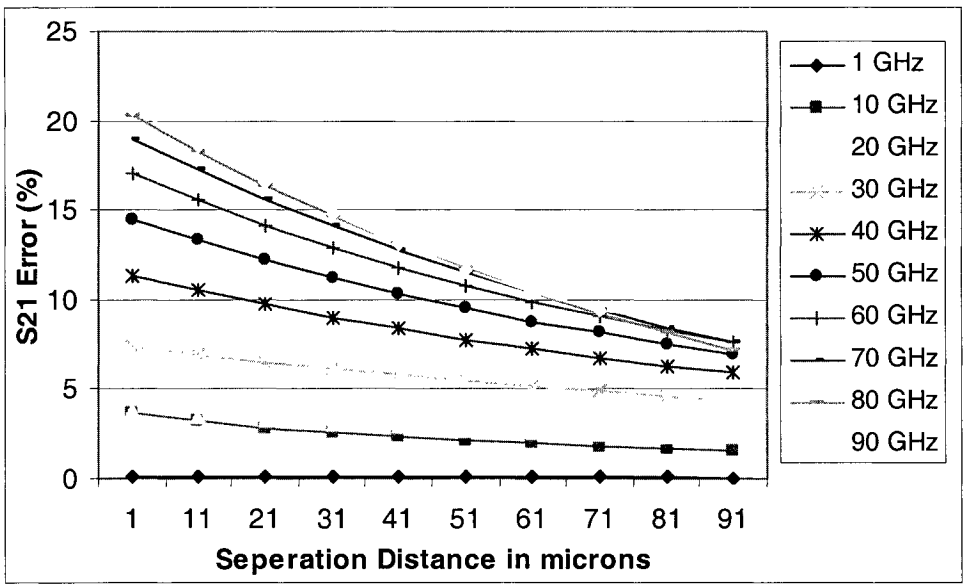

Figure 2-5. Coupling induced error as a function of Separation distance and frequency for the parallel RC circuit.

Based on the above results and discussion and in accordance with the well-known bases of EM theory, some general conclusions regarding coupling can be made:

- The effect of coupling is highly dependant on frequency.
- Coupling magnitude between two components decreases as separation between them increases.

- Coupling in parallel structures is more significant than in series structures.
- Component to Component Coupling has no effect at lower frequencies, even when distance between components is small.

2.2 Electromagnetic Simulators

At millimeter wave frequencies, simulator tools that do not include electromagnetic effects, such as coupling, will not produce accurate results [Yago04]. Furthermore, due to electromagnetic field interaction, the response can be highly geometry dependant. High frequency simulators must take all electromagnetic interactions into account. As an illustrative example consider the Agilent *Advanced Design System* (*ADS*) software [ADS]. First released in 1988 as the *Microwave Design System* (*MDS*), *ADS* evolved through the 90's into a standard tool for Analog and RF circuit design. However as integrated RF and MW designs began to become mainstream, new electromagnetic tools were required to provide accurate simulations. Thus, Agilent introduced *Momentum* to address these ever increasing requirements. *Momentum* ties circuit design together with electromagnetic simulation based on layout. This tool first performs 2 Dimensional (2D) electromagnetic simulation of a specified layout and then can create a model for that layout. Tools such as *Momentum* demonstrate a shift in design methodology. This shift is the increased dependence on electromagnetic numerical tools for verification and design especially when there is evidence of coupling or there is no adequate model available. In the future, there will be increased interdependance between EM solvers and circuit simulators. This is becoming evident with the new releases of Ansoft *Designer* [Ansoft] and Agilent *Momentum* [ADS]. The simulation tools used in this thesis employed electromagnetic numerical methods to evaluate circuit

responses. Common requirements of these tools are to be able to quickly and accurately evaluate the response of a given structure.

Solving electromagnetic problems are no simple task. Depending on the accuracy required, complicated microwave structures can create thousands of variables requiring several Gigabytes of memory to solve [Chun03]. As the complexity and number of variables increases, so too does the amount of time required to solve for the response.

Most electromagnetic tools can be characterized into one of two types: tools that solve Maxwell's equations in differential or in integral form. Electromagnetic simulators that are differential equation (DE) based solve the following differential set of Maxwell's equations [Poza98]:

$$\nabla \times \vec{E} = -\frac{\partial \vec{B}}{\partial t} - \vec{M} \tag{2.2}$$

$$\nabla \times \vec{H} = \frac{\partial \vec{D}}{\partial t} + \vec{J} \tag{2.3}$$

$$\nabla . \vec{D} = \rho_v \tag{2.4}$$

$$\nabla . \vec{B} = 0 \tag{2.5}$$

Whereas tools that are Integral Equation (IE) based, solve the equivalent integral form of Maxwell's equations:

$$\int_C \vec{E} \cdot dl = -\iint_S \frac{\partial \vec{B}}{\partial t} \cdot dS - \iint_S \vec{M} \cdot dS \tag{2.6}$$

$$\int_C \vec{B} \cdot dl = \mu \iint_S \left(\frac{\partial \vec{D}}{\partial t} + \vec{J} \right) \cdot dS \tag{2.7}$$

$$\iint_S \vec{D} \cdot dS = \iiint_V \rho_v \, dV \tag{2.8}$$

$$\iint_S \vec{B} \cdot dS = 0 \tag{2.9}$$

where E is the electric field intensity [V/m], B is the magnetic flux density [T] and D is the electric flux density [C/m^2]. In the integral based equations, S and C represent the surface or the contour over which the given field is to be integrated respectively. J represents the current density [A/m^2] and M, μ, ε, and ρ_v are the magnetic current, permeability, permittivity and volume charge density respectively.

EM simulators need to be able to solve Maxwell's equations. The following tools were used in this thesis for EM simulations:

2.2.1 Sonnet *em*[Sonnet]

Sonnet *em* employs an Integral based method for electromagnetic simulation. In order to solve an electromagnetic structure, appropriate integral equations are drawn and then discretized using Harrington's method of moments (MOM) [Harr68]. The results are matrices that are dense but relatively smaller than Differential Equation based methods. This is due to the fact that the solution space for Differential Equation based methods includes the entire

radiation box whereas an IE based solver like Sonnet *em* confines the solution space to the object only.

Today's IE based EM solvers can be divided into two categories [Raut03]. They are IE-EM solvers using shielded environments or using open environments. Sonnet *em* [Sonnet], Applied Wave Research *Microwave Office* [AWR] and Eagleware *EMPOWER* [Eagleware] are all shielded environment solvers. Agilent *Momentum* [ADS] and Zeland *IE3D* [Zeland] use an open environment, which have infinitely large substrates. The advantage of shielded solvers is that the required numerical analysis is achieved faster [Raut03]. The size of the shielded box must be chosen large enough to accurately simulate the structure and eliminate any coupling to the box wall. Sonnet *em* is considered a planar or 2.5D electromagnetic solver [Raut03] because it solves Maxwell's equations in 2 dimensions and then integrates over the third. When using an open environment, some approximation in integration is required.

For this research Sonnet was used to obtain all electromagnetic data and to verify results. While a single electromagnetic tool cannot be considered the most accurate for every application, Sonnet *em* is an excellent fit in this case because it can produce results faster and with an acceptable degree of accuracy.

2.2.2 Ansoft *High Frequency Structure Simulator*

Ansoft *High Frequency Structure Simulator* (*HFSS*) is a very popular EM solver which employs differential methods to solve Maxwell's equations. *HFSS* is considered a Finite Element technique as the entire volume of the structure is meshed. Thus it is called a 3D EM solver.

2.3 Conclusion

In this chapter, coupling was first defined and then its effect demonstrated through simulation. Coupling was shown to have a major affect on circuit behavior that cannot be ignored at microwave and millimeter wave frequencies. Lastly, full wave electromagnetic tools are introduced. In this thesis, Sonnet *em* is assumed to be accurate and used to generate EM data.

2.4 References

[Abdu01] M. Abdul-Gaffoor, H. Smith, A. Kishk, A. Glisson, "Full wave analysis of electromagnetic coupling in realistic RF multilayer PCB layouts using cascaded parallel plate waveguide model," *Microwave Symposium Digest, 2001 IEEE MTT-S International*, 2001, 1933 – 1936.

[Abdu02] M. Abdul-Gaffoor, H. Smith, A. Kishk, A. Glisson, "Simple and efficient full-wave modeling of electromagnetic coupling in realistic RF multilayer PCB layouts," *IEEE Trans. On Microwave Theory and Tech.*, 2002, 1445 – 1457.

[ADS] *ADS 2004A*, Agilent Technologies, Palo Alto CA, USA.

[AWR] *Microwave Office*, Applied Wave Research, Inc. El Segundo, CA.

[Band93] J. Bandler, S. Chen, R. Biernacki, L. Gao, K. Madsen, H. Yu, "Huber Optimization of Circuits: A Robust Approach," *IEEE Trans. On Microwave Theory and Tech.*, 1994, 2279 – 2287.

[Band94] J. Bandler, R. Biernacki, S. Chen, P. Grobelny, R. Hemmersm, "Space mapping technique for electromagnetic optimization," *IEEE Trans. On Microwave Theory and Tech.*, 1994, 2536 – 2544.

[Cast02] S. Castillo, B. Lail, R. Jedlicka, "Efficient computational models of electromagnetic coupling through general tortuous-path, narrow-slot apertures into shielded systems," *IEEE Antennas and Propagation Society International Symposium*, 2002, 419 – 422.

[Cho99] C. Cho, K. Gupta, "EM-ANN modeling of overlapping open-ends in multilayer microstrip lines for design of bandpass filters," *IEEE Antennas and Propagation Society International Symposium*, 1999, 2592 – 2595.

[Chun03] D. Chun and K. Sabet, "Full-wave Moment Method Simulation of Large-scale Antenna Arrays on High Performance Computing Platforms," *IEEE Antennas and Propagation Society International Symposium*, 2003, 464 – 467.

[Deva01] V. Devabhaktuni, M.C.E. Yagoub, Q. Zhang; "A robust algorithm for automatic development of neural-network models for microwave applications," *IEEE Trans. On Microwave Theory and Tech.*, 2001, 2282 – 2291.

[Deva03] V. Devabhaktuni, B. Chattaraj, M. Yagoub, Q. Zhang, "Advanced microwave modeling framework exploiting automatic model generation, knowledge neural networks, and space mapping," *IEEE Trans. On Microwave Theory and Tech.*, 2003, 1822 – 1833.

[Ding04] X. Ding, V. Devabhaktuni, B. Chattaraj, M.C.E. Yagoub, M. Deo, J. Xu, Q. Zhang, "Neural-Network Approaches to Electromagnetic-Based Modeling of Passive Components and Their Applications to High-Frequency and High-Speed Nonlinear Circuit Optimization," *IEEE Trans. On Microwave Theory and Tech.*, 2004, 436-449.

[Eagleware] *EMPOWER/ML*, Eagleware-Elanix corp., Norcross, GA.

[Erdi00] I. Erdin, M. Nakhla, R. Achar, "Circuit analysis of electromagnetic radiation and field coupling effects for networks with embedded full-wave modules," *IEEE Trans. On Electromagnetic Compatibility*, 2000, 449 – 460.

[Gupt81] K. Gupta, R. Garg, R. Chadha, *Computer Aided Design of Microwave Circuits*, Dedham MA, Artech House Inc., 1981.

[Harr68] R. F. Harrington, *Field computation by moment methods*, New York: Macmillan, 1968.

[HFSS] Ansoft-*HFSS* v.8.0, Ansoft Corp., Pittsburg, PA.

[Lail02] B. Lail, S. Castillo, "A hybrid MoM/FEM model of coupling to thin-wire structures in complex cavities," *IEEE Antennas and Propagation Society International Symposium*, 2002, 290 – 293.

[Ozde03] M. Ozdemir, H. Arslan, E. Arvas, "Mutual coupling effect in multiantenna wireless communication systems," *IEEE GLOBECOM Global Telecommunications Conference*, 2003, 829 – 833.

[Poza98] D. Pozar, *Microwave Engineering*, 2nd ed. New York: John Wiley & Sons Inc., 1998.

[Raut03] J. Rautio, "Planar electromagnetic analysis," *IEEE Microwave Magazine*, 2003, 35 – 41.

[Rizz04] V. Rizzoli, A. Costanzo, D. Masotti, A. Lipparini, F. Mastri, "Computer-aided optimization of nonlinear microwave circuits with the aid of electromagnetic simulation," *IEEE Trans. On Microwave Theory and Tech.*, 2004, 362 – 377.

[Yago04] M.C.E. Yagoub, P. Sharma, "Characterization of EM effects in RF/microwave integrated circuits," *34th European Microwave Conf. (2004)*, Amsterdam, Netherlands, 221-224.

[Sonnet] Sonnet *em* 9.52, Sonnet Software Inc., Liverpool, NY.

[Xu03] J. Xu, M.C.E. Yagoub, R. Ding, Q. Zhang, "Exact adjoint sensitivity analysis for neural-based microwave modeling and design," *IEEE Trans. On Microwave Theory and Tech.*, 2003, 226 – 237.

[Zeland] *IE3D*, Zeland Software, Inc., Fermont, CA.

[Zhan03] Q. Zhang, F. Wang, V. Devabhaktuni, "Neural network structures for EM/microwave modeling," *IEEE Antennas and Propagation Society International Symposium*, 1999, 2576 – 2579.

[Zhao98] J. Zhao, J. Fang, "Validity of Mutual Inductor Model for Electromagnetic Coupling between Vias in Integrated-Circuit Packages and Printed Circuit Boards," *IEEE Electronic Components and Technology Conference*, 1998, 1083 – 1088.

CHAPTER III

TECHNIQUES FOR MODELING COUPLING

This chapter presents techniques for modeling coupling for all types of circuit configurations. Modeling for series and parallel connected networks are considered first, and second a more general method for modeling coupling using the Connection Scattering Matrix [Gupt81] is detailed. The chapter concludes by considering the limitations of the proposed approach along with a practical example of using coupling models in optimization.

Generally speaking, coupling models are separate components that are inserted into the network to account for mutual and distributed coupling between two components. A simple example of a two port series network is shown in figure 3-1 which demonstrates both mutual and distributed coupling in a network consisting of two arbitrary components A and B connected by a interconnect I.

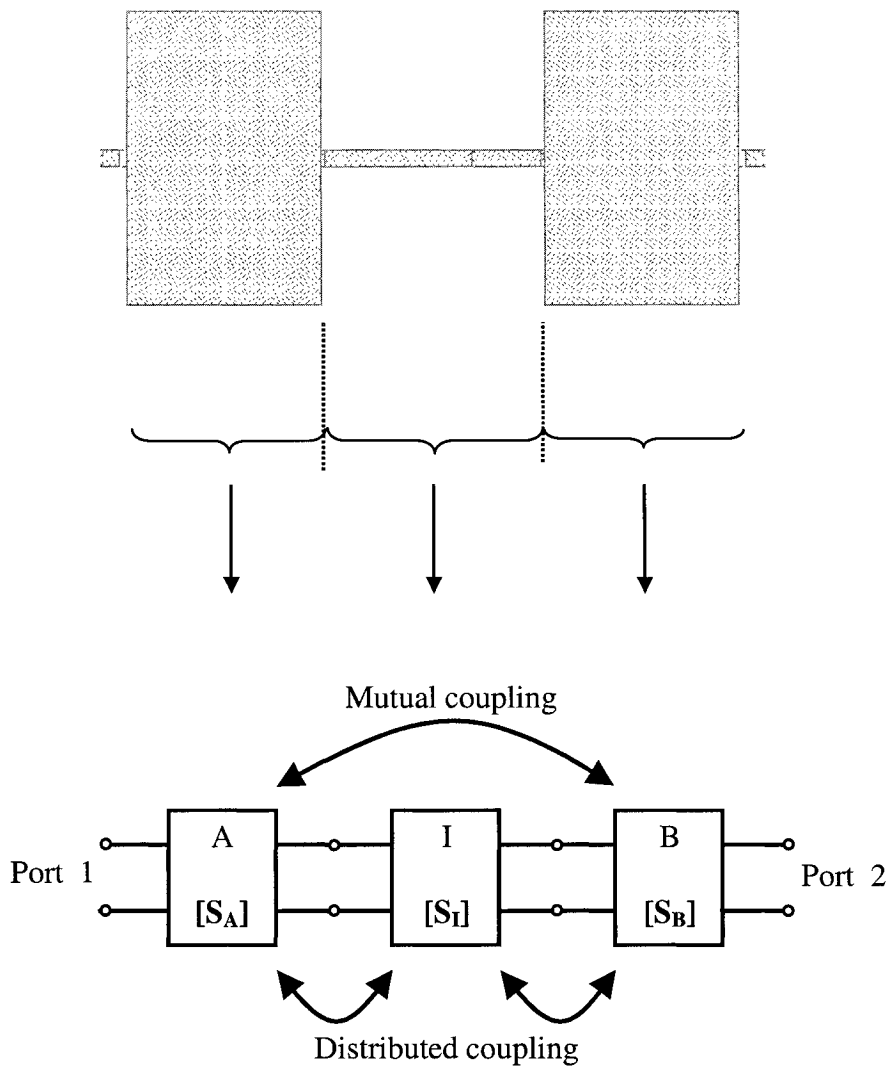

Figure 3-1. Simple 2-port series network.

where A and B are arbitrary components and I is the interconnect between them.

The coupling model can be derived given the network's overall S-parameters as well as each component's S-parameters. In this example, a coupling model $[C_{AB}]$ will replace the overall effect of the Interconnect (I) S-parameters, the Mutual coupling between A and B and the Distributed coupling between the components and the interconnect.

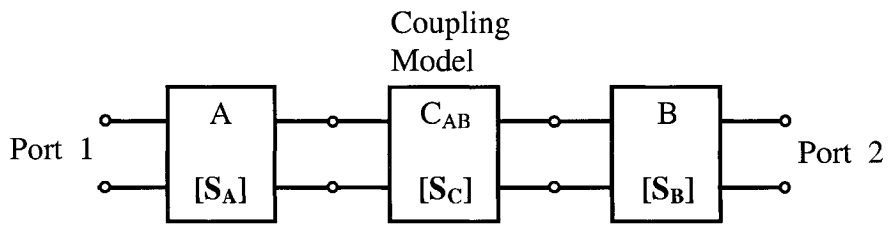

Figure 3-2. Simple 2-port network modified by adding the coupling model.

C_{AB} represents the coupling model between components A and B with scattering matrix $[S_C]$.

Coupling models can be inserted in series and in parallel depending on which type of network is considered. The mathematical solution for the S-parameters that characterize such coupling models is different for each type network. Because the proposed approaches are based on mathematical manipulations of both the *S*- and *T*-matrices, a review of the basic properties of such characteristic matrices is necessary. We will complete this overview by the Connection Scattering Matrix [Gupt81] which is essential to compute the overall scattering matrix of complex high frequency integrated systems.

3.1 Characteristic Matrices And Their Properties

3.1.1 Scattering Parameter Matrices

An *n*-port network has *n* external connections into which power can be fed and from which power can be taken. In general, power can get from any port (as input) to any other port (as output). There are thus *n* incoming (incident) wave complex amplitudes usually designated by the *n* complex quantities a_n and *n* outgoing (reflected) wave complex quantities designated by

the n complex quantities b_n. The corresponding n-vectors **[a]** and **[b]** are related by the following relation

$$\begin{bmatrix} b_1 \\ \vdots \\ b_n \end{bmatrix} = \begin{bmatrix} S_{11} & \cdots & S_{1n} \\ \vdots & \ddots & \vdots \\ S_{n1} & \cdots & S_{nn} \end{bmatrix} \begin{bmatrix} a_1 \\ \vdots \\ a_n \end{bmatrix} \tag{3.1}$$

where **[S]** is an n-by-n square matrix of complex numbers called the scattering matrix, whose elements are termed "S-parameters". If the network has internal independent generators, a wave vector **[c]** must be included as

$$\mathbf{[b] = [S]\,[a] + [c]} \tag{3.2}$$

Figure 3-3 illustrates the case of a two-port network, showing the related incident and reflected waves.

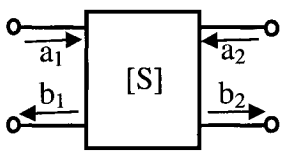

Figure 3-3. A two-port network representation with the related incident and reflected waves.

3.1.2 Transfer Matrix

Let us consider any passive based n-port system. Since it can be defined as a combination of series and/or parallel individual devices, its overall characteristic matrix can be conveniently obtained from the individual device matrices using the transfer scattering-parameters or simply the T-parameters ([Fric94], [Gupt81]). As for the S-parameters, the T-parameters are defined as function of the incident and reflected waves as

$$\begin{bmatrix} b_1 \\ a_1 \end{bmatrix} = \begin{bmatrix} T_{11} & T_{12} \\ T_{21} & T_{22} \end{bmatrix} \begin{bmatrix} a_2 \\ b_2 \end{bmatrix} \tag{3.3}$$

Relationships for converting from S-parameters to T-parameters and vice-versa are given by the following relations [Gupt81]:

$$T_{11} = \frac{-S_{11}S_{22} + S_{12}S_{21}}{S_{21}} \tag{3.4a}$$

$$T_{12} = \frac{S_{11}}{S_{21}} \tag{3.4b}$$

$$T_{21} = \frac{-S_{22}}{S_{21}} \tag{3.4c}$$

$$T_{22} = \frac{1}{S_{21}} \tag{3.4d}$$

and

$$S_{11} = \frac{T_{12}}{T_{22}} \tag{3.5a}$$

$$S_{12} = T_{11} - \frac{T_{12}T_{21}}{T_{22}} \tag{3.5b}$$

$$S_{21} = \frac{1}{T_{22}} \tag{3.5c}$$

$$S_{22} = -\frac{T_{21}}{T_{22}} \tag{3.5d}$$

This concept can be applied in the de-embedding process. Let us consider a device under test (DUT) to be characterized. The classical way to determine its scattering matrix is to insert it in a fixture and measure the overall matrix. Since the fixtures are known and overall matrix is known, the DUT's S-parameters can then be found by de-embedding. This concept will be later applied to EM coupling. Figure 3-4 demonstrates a two-port system represented by three cascaded two-port sub-networks connected in series where device B is a DUT.

After converting all parameters in Fig. 3-4 to *T*-parameters, the total system response can be described as follows:

$$\begin{bmatrix} T_{11}^T & T_{12}^T \\ T_{21}^T & T_{22}^T \end{bmatrix} = \begin{bmatrix} T_{11}^A & T_{12}^A \\ T_{21}^A & T_{22}^A \end{bmatrix} \begin{bmatrix} T_{11}^X & T_{12}^X \\ T_{21}^X & T_{22}^X \end{bmatrix} \begin{bmatrix} T_{11}^C & T_{12}^C \\ T_{21}^C & T_{22}^C \end{bmatrix}$$

$$\Rightarrow \qquad [\mathbf{T_T}] = [\mathbf{T_A}] * [\mathbf{T_X}] * [\mathbf{T_C}] \tag{3.6}$$

where $[\mathbf{T_T}]$ is the *T*-matrix for the whole system, while $[\mathbf{T_A}]$, $[\mathbf{T_X}]$, and $[\mathbf{T_C}]$ are the *T*-matrices of the three cascaded sub-networks, namely, A, B, and C, respectively.

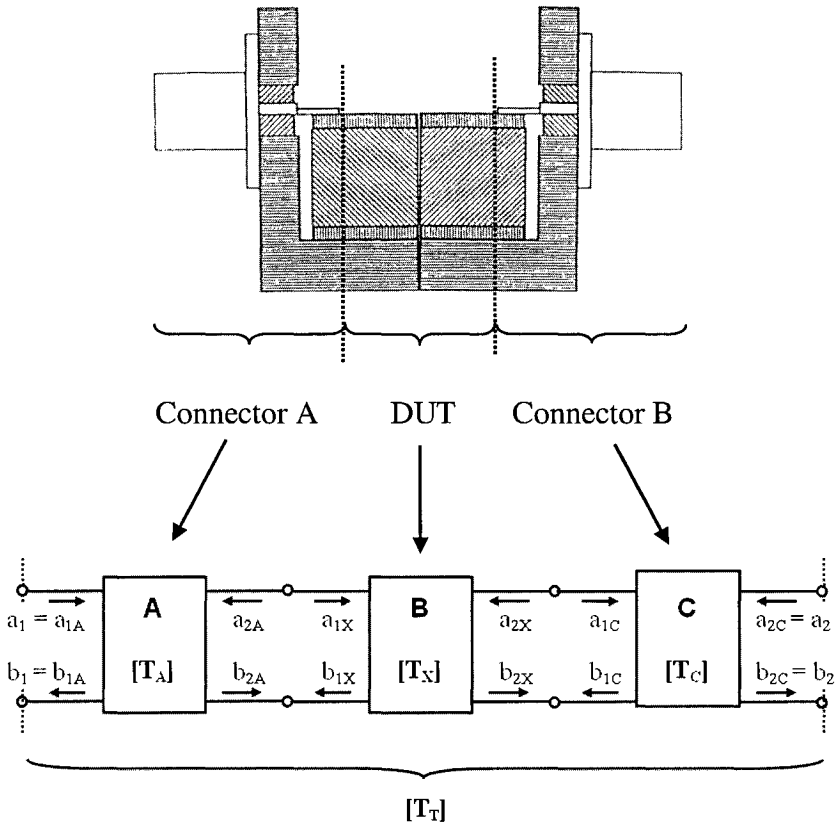

Figure 3-4. Schematization of a fixture modeled as a set of three two-port sub-networks connected in series. B is the DUT which $[\mathbf{T_X}]$ matrix needs to be extracted. A and C could represent the fixture input/output transmission lines, the connectors, etc.

Since device B is the DUT to be characterized, its *T*-matrix $[\mathbf{T_X}]$ could be extracted from [Chen01]. Thus,

$$T_{11}^{X} = \frac{-(-T_{22}^{A}T_{22}^{C}T_{11}^{T} + T_{22}^{A}T_{21}^{C}T_{12}^{T} + T_{12}^{A}T_{22}^{C}T_{21}^{T} - T_{12}^{A}T_{21}^{C}T_{22}^{T})}{(T_{12}^{A}T_{21}^{A} - T_{11}^{A}T_{22}^{A})(T_{12}^{C}T_{21}^{C} - T_{11}^{C}T_{22}^{C})} \tag{3.7a}$$

$$T_{12}^{X} = \frac{(-T_{22}^{A}T_{12}^{C}T_{11}^{T} + T_{22}^{A}T_{11}^{C}T_{12}^{T} + T_{12}^{A}T_{12}^{C}T_{21}^{T} - T_{12}^{A}T_{11}^{C}T_{22}^{T})}{(T_{12}^{A}T_{21}^{A} - T_{11}^{A}T_{22}^{A})(T_{12}^{C}T_{21}^{C} - T_{11}^{C}T_{22}^{C})} \quad (3.7b)$$

$$T_{21}^{X} = \frac{(-T_{21}^{A}T_{22}^{C}T_{11}^{T} + T_{21}^{A}T_{21}^{C}T_{12}^{T} + T_{11}^{A}T_{22}^{C}T_{21}^{T} - T_{11}^{A}T_{21}^{C}T_{22}^{T})}{(T_{12}^{A}T_{21}^{A} - T_{11}^{A}T_{22}^{A})(T_{12}^{C}T_{21}^{C} - T_{11}^{C}T_{22}^{C})} \quad (3.7c)$$

$$T_{22}^{X} = \frac{(T_{21}^{A}T_{12}^{C}T_{11}^{T} - T_{21}^{A}T_{11}^{C}T_{12}^{T} - T_{11}^{A}T_{12}^{C}T_{21}^{T} + T_{11}^{A}T_{11}^{C}T_{22}^{T})}{(T_{12}^{A}T_{21}^{A} - T_{11}^{A}T_{22}^{A})(T_{12}^{C}T_{21}^{C} - T_{11}^{C}T_{22}^{C})} \quad (3.7d)$$

This result is mathematically similar to the work developed by Chen and Deen [Chen01] who simulated a two-port system with open and short configurations and then mathematically de-embedded the DUT. We now extend this method to model coupling in lumped components.

3.2 Evaluation of Coupling in Series Connected Networks

To illustrate the application of this concept to coupling in series connected networks, let us consider two sub-networks A and B connected in series via a transmission line or interconnect I (Fig. 3-5). As shown in the above section, a classical approach of finding the overall response $[\mathbf{T_T}]$ of these cascaded components would be to simply combine the first sub-network, the interconnect and the second sub-network *T*-parameters together using (3.6),

$$[\mathbf{T_T}] = [\mathbf{T_A}] * [\mathbf{T_I}] * [\mathbf{T_B}] \quad (3.8)$$

The above relation is valid only if we do not consider the distributed electromagnetic coupling between contiguous elements. In fact, since coupling is related to electromagnetic field interaction between the components, the matrix $[\mathbf{T_T}]$ cannot be accurately evaluated through (3.8).

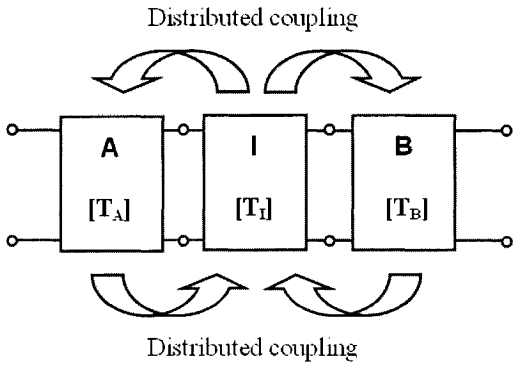

Figure 3-5. Distributed electromagnetic coupling between contiguous sub-networks. I is the interconnect characterized by its *T*-matrix $[\mathbf{T_I}]$ while the matrices of the two sub-networks A and B are $[\mathbf{T_A}]$ and $[\mathbf{T_B}]$ respectively.

The aim of the proposed method is to find out how to model this electromagnetic coupling knowing that this quantity is almost impossible to measure and very difficult to evaluate [Yago04], [Frid98], [Baud97] and [Yin03].

We propose to include the electromagnetic coupling as an extra sub-network between any two components in series. Therefore, the network shown in Fig. 3-5 would be modified to the one shown in Fig. 3-6. The procedure for characterizing the sub-networks EMC1 and EMC2 in the above figure is to compare the following *T*-matrices of the whole network.

$$[T_{T\ \text{without coupling}}] = [T_A] * [T_I] * [T_B] \quad (3.9)$$

$$[T_{T\ \text{with coupling}}] = [T_A] * [T_{X1}] * [T_I] * [T_{X2}] * [T_B] \quad (3.10)$$

The first matrix $[T_{T\ \text{without coupling}}]$ could be obtained through individual simulation or measurements of the individual matrices $[T_A]$, $[T_I]$, and $[T_B]$, while the second matrix $[T_{T\ \text{with coupling}}]$ is obtained by evaluating the real network response.

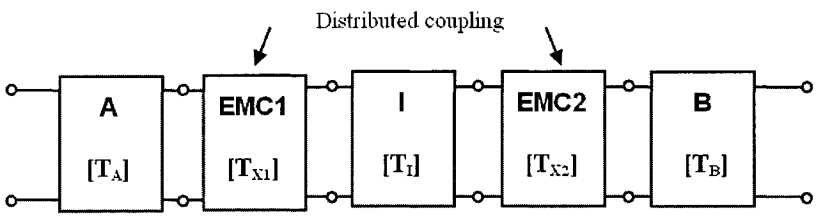

Figure 3-6. Modified topology of the network shown in Fig. 3-5, replacing the electromagnetic coupling by two-port networks of matrices $[T_{X1}]$ and $[T_{X2}]$ in series with the sub-networks A and B.

A general procedure to extract the coupling between two components can be stated as:

***Step* 1** Simulate the individual components including interconnects to obtain $[S_A]$, $[S_I]$, and $[S_B]$. Convert to *T*-parameters to obtain $[T_A]$, $[T_I]$, and $[T_B]$.

***Step* 2** Simulate all two-by-two combinations of the components to obtain $[S_{AI}]$ and $[S_{IB}]$. Convert to *T*-parameters to obtain $[T_{AI}]$ and $[T_{IB}]$ defined as

$$[T_{AI}] = [T_A] * [T_I] \quad (3.11)$$

$$[T_{IB}] = [T_I] * [T_B] \quad (3.12)$$

***Step* 3** Measure all two-by-two combinations of the components to obtain $[S_{ACI}]$ and $[S_{ICB}]$. Convert to *T*-parameters to obtain $[T_{ACI}]$ and $[T_{ICB}]$ defined as

$$[T_{ACI}] = [T_A] * [T_{X1}] * [T_I] \quad (3.13)$$

$$[T_{ICB}] = [T_I] * [T_{X2}] * [T_B] \quad (3.14)$$

***Step* 4** Measure the overall device *S*-parameters and convert to *T*-parameters to obtain $[T_{T\ \text{with coupling}}]$.

***Step* 5** Use (3.9) to get $[T_{T\ \text{without coupling}}]$.

***Step* 6** Use (3.7), (3.10) - (3.14) to compute the coupling, i.e., the $[T_{X1}]$ and $[T_{X2}]$ matrices.

3.3 Evaluation of Coupling in Parallel Connected Networks

For parallel structures, *Y*-parameters are used instead of *T*-parameters to calculate the effect of coupling and derive corresponding models. For instance, for a parallel Resistor Inductor network, the same approach is used: The coupling component will be inserted in parallel with the existing components. For instance, its Y_{11X} parameter is given by:

$$Y_{11X} = Y_{11\_RL\_Ac} - Y_{11\_R} - Y_{11\_L} \quad (3.15)$$

where $[\mathbf{Y_{RL\_Ac}}]$, $[\mathbf{Y_R}]$, and $[\mathbf{Y_L}]$ are the admittance matrices of the entire circuit, the Resistor and the Inductor, respectively. Note that in our circuit code, all bends and transmission lines are accounted for. The other *Y*-parameters are calculated in a similar manner.

3.4 Evaluation of Coupling in Arbitrarily Connected Networks

For circuits that branch or have connections to ground, the previous formulations for series and parallel connected networks cannot be used to evaluate the coupling. A convenient method to extend this research to arbitrarily connected networks is the well known Connection Scattering Matrix representation as given by Gupta [Gupt81] and first referenced by Monaco [Mona74].

Given that port #*i* of a sub-network is connected to the port #*j* of another sub-network in cascade, a 2x2 connection matrix can be created that describes the relation between the related incoming and outgoing waves [Gupt81],

$$\begin{bmatrix} b_i \\ a_j \end{bmatrix} = \begin{bmatrix} 0 & 1 \\ 1 & 0 \end{bmatrix} \begin{bmatrix} a_i \\ b_j \end{bmatrix} \tag{3.16}$$

By generalization to all existing connections inside the *n*-port network, we obtain the *nxn* connection matrix $[\Gamma]$ that describes the entire network topology

$$\mathbf{[b] = [\Gamma]\,[a]} \tag{3.17}$$

Substituting for **[b]** in (3.2) and solving for **[a]**, gives

$$[\Gamma]\,[a] = [S]\,[a] + [c] \quad \Rightarrow [a] = \{\,[\Gamma] - [S]\,\}^{-1}\,[c] \tag{3.18}$$

Substituting back into (3.17) gives

$$[b] = [\Gamma]\,\{\,[\Gamma] - [S]\,\}^{-1}\,[c] \tag{3.19}$$

The matrix $[W] = \{\,[\Gamma] - [S]\,\}^{-1}$ is called the connection scattering matrix that depends only on the network topology. It allows us to determine the incoming wave vector **[a]**, and then, using (3.19), the outgoing wave vector **[b]**. Hence, the overall characteristic matrix of the entire network can be totally defined by

$$[b] = [S_T]\,[a] \tag{3.20}$$

Evaluation of coupling using *T*-parameters is only possible for cascaded networks. For other types of networks, a new formulation is necessary. Using the Connection Scattering Matrix representation, a generic extendible procedure can be developed to model coupling in any type of *n*-port sub-network. For example, to model the coupling in the T-Connected circuit shown in Fig. 3-7 and defined by matrix $[S_m]$, a three-port device EMC of scattering matrix $[S_X]$ has to be inserted in the circuit layout at the T-Junction node. Therefore, we assume that $[S_X]$ is unknown while all other two-port blocks are well characterized through their *S*-parameters.

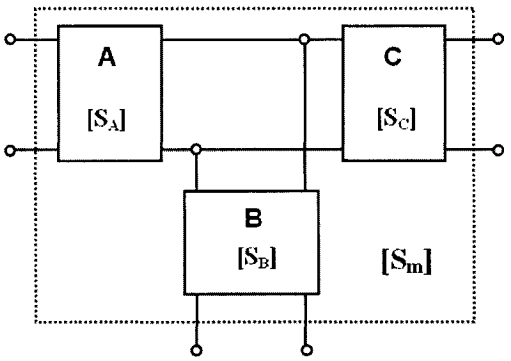

(a)

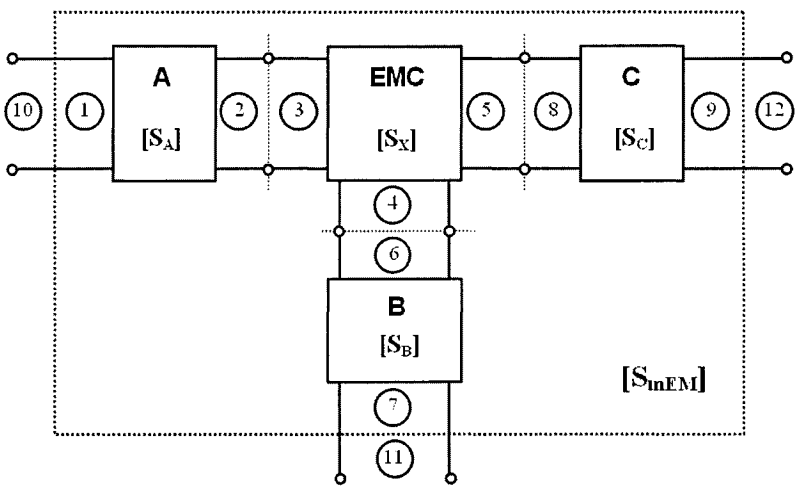

(b)

Figure 3-7. T-Junction network:

(a) Original configuration with the three networks A, B, and C.

(b) Modified circuit including the three-port coupling sub-network EMC and the port numbering.

For the whole structure and following the port numbering, the connection matrix [Γ] is of form

$$[\Gamma]=\begin{bmatrix}
0&0&0&0&0&0&0&0&0&1&0&0\\
0&0&1&0&0&0&0&0&0&0&0&0\\
0&1&0&0&0&0&0&0&0&0&0&0\\
0&0&0&0&0&1&0&0&0&0&0&0\\
0&0&0&0&0&0&0&1&0&0&0&0\\
0&0&0&1&0&0&0&0&0&0&0&0\\
0&0&0&0&0&0&0&0&0&0&1&0\\
0&0&0&0&1&0&0&0&0&0&0&0\\
0&0&0&0&0&0&0&0&0&0&0&1\\
1&0&0&0&0&0&0&0&0&0&0&0\\
0&0&0&0&0&0&1&0&0&0&0&0\\
0&0&0&0&0&0&0&0&1&0&0&0
\end{bmatrix} \tag{3.21}$$

and the related $[\mathbf{S}_{\mathbf{mEM}}]$ matrix containing all individual S matrices is equal to

$$[\mathbf{S}_{\mathbf{mEM}}]=\begin{bmatrix}
S_{11}^{A}&S_{12}^{A}&0&0&0&0&0&0&0&0&0&0\\
S_{21}^{A}&S_{22}^{A}&0&0&0&0&0&0&0&0&0&0\\
0&0&S_{11}^{X}&S_{12}^{X}&S_{13}^{X}&0&0&0&0&0&0&0\\
0&0&S_{21}^{X}&S_{22}^{X}&S_{23}^{X}&0&0&0&0&0&0&0\\
0&0&S_{31}^{X}&S_{32}^{X}&S_{33}^{X}&0&0&0&0&0&0&0\\
0&0&0&0&0&S_{11}^{B}&S_{12}^{B}&0&0&0&0&0\\
0&0&0&0&0&S_{21}^{B}&S_{22}^{B}&0&0&0&0&0\\
0&0&0&0&0&0&0&S_{11}^{C}&S_{12}^{C}&0&0&0\\
0&0&0&0&0&0&0&S_{21}^{C}&S_{22}^{C}&0&0&0\\
0&0&0&0&0&0&0&0&0&0&0&0\\
0&0&0&0&0&0&0&0&0&0&0&0\\
0&0&0&0&0&0&0&0&0&0&0&0
\end{bmatrix} \tag{3.22}$$

Therefore, equation (3.19) gives

$$\begin{bmatrix} b_1 \\ b_2 \\ b_3 \\ b_4 \\ b_5 \\ b_6 \\ b_7 \\ b_8 \\ b_9 \\ b_{10} \\ b_{11} \\ b_{12} \end{bmatrix} = \begin{bmatrix} 0 & 0 & 0 & 0 & 0 & 0 & 0 & 0 & 0 & 1 & 0 & 0 \\ 0 & 0 & 1 & 0 & 0 & 0 & 0 & 0 & 0 & 0 & 0 & 0 \\ 0 & 1 & 0 & 0 & 0 & 0 & 0 & 0 & 0 & 0 & 0 & 0 \\ 0 & 0 & 0 & 0 & 0 & 1 & 0 & 0 & 0 & 0 & 0 & 0 \\ 0 & 0 & 0 & 0 & 0 & 0 & 0 & 1 & 0 & 0 & 0 & 0 \\ 0 & 0 & 0 & 1 & 0 & 0 & 0 & 0 & 0 & 0 & 0 & 0 \\ 0 & 0 & 0 & 0 & 0 & 0 & 0 & 0 & 0 & 0 & 1 & 0 \\ 0 & 0 & 0 & 0 & 1 & 0 & 0 & 0 & 0 & 0 & 0 & 0 \\ 0 & 0 & 0 & 0 & 0 & 0 & 0 & 0 & 0 & 0 & 0 & 1 \\ 1 & 0 & 0 & 0 & 0 & 0 & 0 & 0 & 0 & 0 & 0 & 0 \\ 0 & 0 & 0 & 0 & 0 & 0 & 1 & 0 & 0 & 0 & 0 & 0 \\ 0 & 0 & 0 & 0 & 0 & 0 & 0 & 0 & 1 & 0 & 0 & 0 \end{bmatrix}$$

$$\begin{bmatrix} -S_{11}^A & -S_{12}^A & 0 & 0 & 0 & 0 & 0 & 0 & 0 & 1 & 0 & 0 \\ -S_{21}^A & -S_{22}^A & 1 & 0 & 0 & 0 & 0 & 0 & 0 & 0 & 0 & 0 \\ 0 & 1 & -S_{11}^X & -S_{12}^X & -S_{13}^X & 0 & 0 & 0 & 0 & 0 & 0 & 0 \\ 0 & 0 & -S_{21}^X & -S_{22}^X & -S_{23}^X & 1 & 0 & 0 & 0 & 0 & 0 & 0 \\ 0 & 0 & -S_{31}^X & -S_{32}^X & -S_{33}^X & 0 & 0 & 1 & 0 & 0 & 0 & 0 \\ 0 & 0 & 0 & 1 & 0 & -S_{11}^B & -S_{12}^B & 0 & 0 & 0 & 0 & 0 \\ 0 & 0 & 0 & 0 & 0 & -S_{21}^B & -S_{22}^B & 0 & 0 & 0 & 1 & 0 \\ 0 & 0 & 0 & 0 & 1 & 0 & 0 & -S_{11}^C & -S_{12}^C & 0 & 0 & 0 \\ 0 & 0 & 0 & 0 & 0 & 0 & 0 & -S_{21}^C & -S_{22}^C & 0 & 0 & 1 \\ 1 & 0 & 0 & 0 & 0 & 0 & 0 & 0 & 0 & 0 & 0 & 0 \\ 0 & 0 & 0 & 0 & 0 & 0 & 1 & 0 & 0 & 0 & 0 & 0 \\ 0 & 0 & 0 & 0 & 0 & 0 & 0 & 0 & 1 & 0 & 0 & 0 \end{bmatrix}^{-1} \begin{bmatrix} 0 \\ 0 \\ 0 \\ 0 \\ 0 \\ 0 \\ 0 \\ 0 \\ 0 \\ c_{10} \\ c_{11} \\ c_{12} \end{bmatrix}$$

(3.23)

Since **[S_X]** is unknown, we must rearrange the above equation and solve, under the following conditions for vectors **[b]** and **[c]**

$$
\begin{aligned}
&\text{if } c_{10}=1, c_{11}=0, c_{12}=0 \\
&\text{then } b_1=S_{11}^T, b_7=S_{21}^T, b_9=S_{31}^T \\
&\text{if } c_{10}=0, c_{11}=1, c_{12}=0 \\
&\text{then } b_1=S_{12}^T, b_7=S_{22}^T, b_9=S_{32}^T \\
&\text{if } c_{10}=0, c_{11}=0, c_{12}=1 \\
&\text{then } b_1=S_{13}^T, b_7=S_{23}^T, b_9=S_{33}^T
\end{aligned}
\tag{3.24}
$$

Although all the operations are straightforward, their manipulation is complex. So, the system was implemented in the algebra language MAPLE [Maple]. Solving for the overall circuit *S*-parameters gives a system of nine equations as shown in Appendix I. The matrix $[\mathbf{S_X}]$ can be now accurately obtained (see Appendix II).

The advantage of the above technique is its accuracy (no simplification or approximation was made to derive the equations) and its ease of implementation in a circuit simulator.

3.5 Limitations of the proposed approach

As is true with most engineering problems, no single method can be adequate for every type of problem encountered. The results shown later demonstrate that there are some sources of error in this approach, especially above 65GHz.

First, while the proposed method is accurate for all directly adjacent component to component coupling, coupling to non-adjacent components in separate sub-networks is ignored, and therefore, will introduce error. These errors tend to occur as signal wavelength

becomes shorter. Thus in high millimeter wave frequencies, non-adjacent components exert more and more coupling effect. Some effort has been taken to model this effect, however the results were not sufficiently accurate.

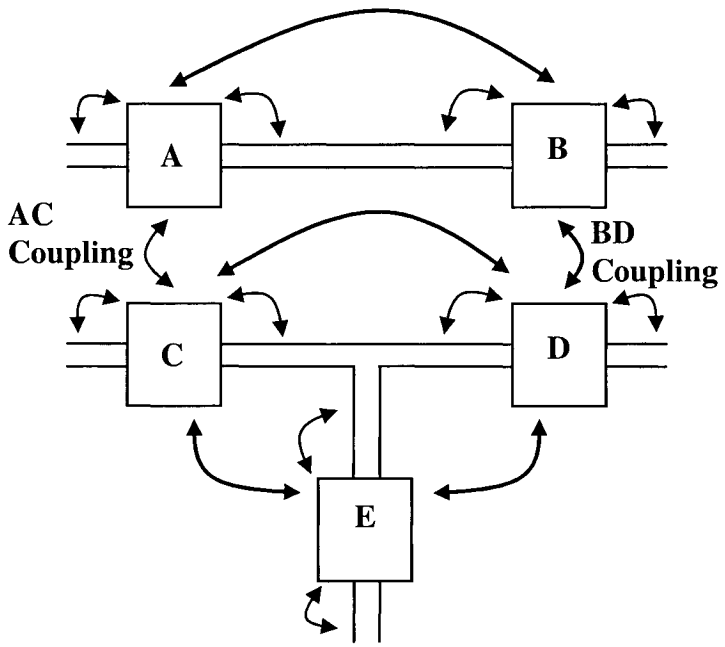

Figure 3-8. A Three component circuit showing all sorts of adjacent and non-adjacent coupling effects. Sub-networks A-B and C-D-E can couple causing error.

In the above figure, the presence of sub-network A-B exerts some influence on the sub-network C-D-E. Simply ignoring sub-network A-B to measure the coupling in C-D-E is not accurate since the electromagnetic fields of sub-network A-B can also couple to sub-network C-D-E. We can account for this coupling by assuring that there is adequate distance between the sub-networks for the coupling components to be used with accurate results.

The second limitation of this approach concerns how quickly the simulation can be performed. Using our approach, many smaller simulations will be performed instead of a single larger simulation of the whole structure. Sonnet [Sonnet] predicts that simulation time is proportional to the cube of the number of subsections. A significant simulation time reduction can be achieved if a large circuit is broken into two smaller sub-circuits at the cost of accuracy due to coupling. However, because Sonnet *em* uses a shielded environment, reference planes must be inserted in order to avoid coupling to the edge of the box. We have found in our simulations in sonnet *em*, that coupling to the box wall can be avoided if there is sufficient separation between the box wall and the structure being simulated. Employing reference planes can safely avoid this undesirable coupling as well as any effects of port discontinuities as shown below.

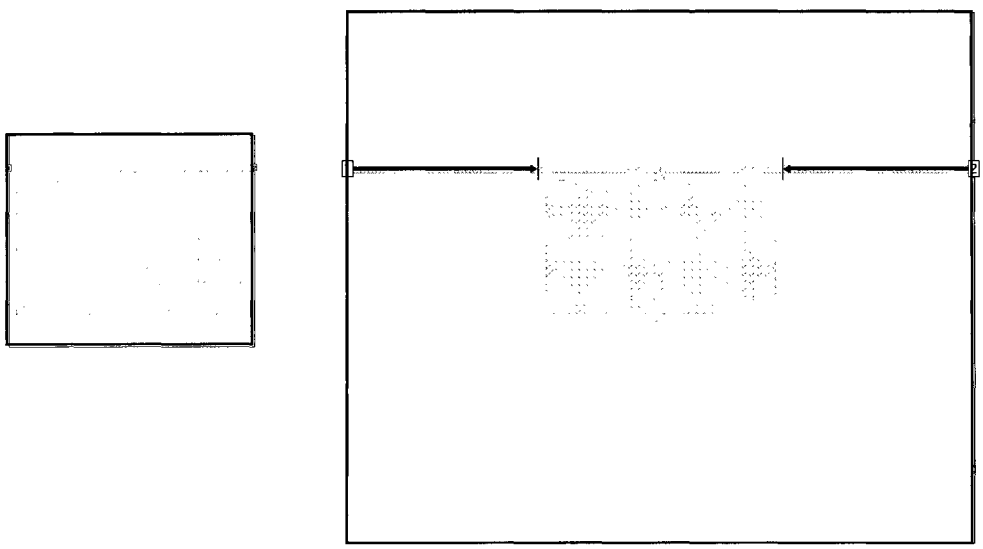

Figure 3-9. Example of simulations without reference planes (fig.3-9a) and with reference planes (fig.3-9b). The black outline is Sonnet 'metal box wall'.

While increasing simulation box size increased the simulation accuracy, it has also reduced the efficiency especially with respect to the Matrix fill time which is an indication of how long calculations take internal to Sonnet *em*. In order to demonstrate this, consider a 2nd order filter composed of 2 capacitors and 2 inductors.

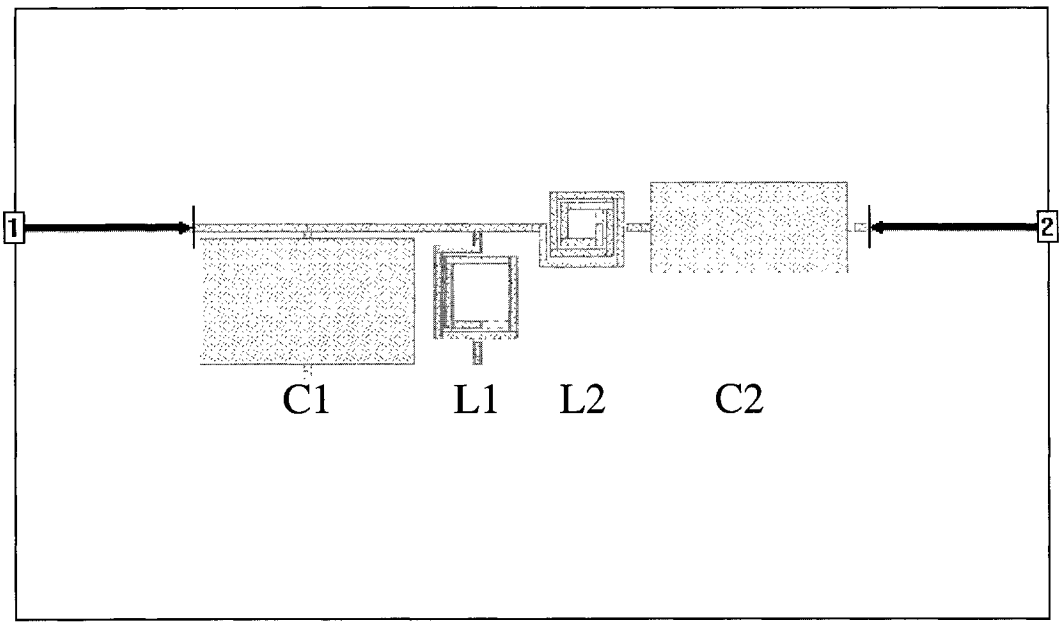

Figure 3-10. 2nd order filter simulation.

From table 3-1, shown below, it is clear that because of the overhead cost of inserting reference planes, our method for using coupling component cannot find use as a tool to speed up a single simulation. Using the figures given, to determine a single simulation result using the proposed coupling tools would take 404s per frequency as opposed to 96s per frequency in a single run simulation. If we simulate each component individually with reference planes, the complete simulation would take 202s and without reference planes 28s per frequency.

Table 3-1. Simulation time needed for the circuit shown in figure 3-10.

Component	Number of Subsections	Memory Required (MB)	Matrix Fill time	Total time per frequency
C1 small(fig.3-9a)	161	3	5s	6s
C1 large(fig.3-9b)	167	9	39s	45s
L1	351	8	58s	65s
L2	273	8	36s	42s
C2	153	9	44s	50s
C1-L1	481	12	69s	76s
L1-L2	587	12	72s	79s
L2-C2	393	12	40s	47s
Filter (fig. 3-10)	837	23	91s	96s

One might ask how coupling models can be useful if they do not offer any advantages in terms of simulation speed. The answer lies in the fact that we can perform all the simulations required to calculate the coupling models off-line. This can permit the creation of a library of components to be used. Once implemented in a circuit simulator, the resulting simulation time/frequency is approximately 1/30s in a circuit simulator as opposed to 96s in Sonnet *em*. This represents the first time that lumped models have been implemented in a circuit simulator including separate individual models for the effect of coupling. Secondly, if it is necessary to consider more than one possible value for each component, this approach can realize enormous time savings. The reason this is true is because each time one component in a network is adjusted, the entire network does not need to be re-simulated. Each component can

be assumed to interact only with adjacent components and through the use of the coupling components this remains largely accurate. The obvious application of this approach is optimization, and other possible applications could be design automation, design modification and yield optimization.

The goal of this section was to demonstrate that these limitations have been considered and accounted for. The first limitation, namely non-adjacent coupling error can be mitigated through careful layout design. Regarding speed, it was shown that dramatic time savings if model S-parameters have been created off-line. This will become ever more evident when we consider Discrete Optimization.

3.6 Discrete Optimization Using Coupling Models

Using our method for modeling coupling, efficient discrete optimization of millimeter wave circuits can be achieved with high levels of accuracy. Here, discrete optimization refers to an optimization with discrete variables. The usage of continuous variables is not in the scope of this thesis, since it will require continuous models for lumped components and coupling models. Essentially, large simulations can be broken into smaller pieces and independently evaluated while maintaining full accuracy by including the effects of coupling.

Subdividing a circuit to perform simulations more quickly is not a novel concept. However by using coupling models, simulation accuracy is kept high by including the effects of coupling. It is useful to examine recent research to fully understand the difference between

the proposed approach and currently available literature. The main problem when considering EM optimization is simulation time. Optimization naturally implies simulation of different structures to determine an optimum solution. In many cases, random starting points are required in an optimization process. There are three main methods used to reduce the amount of simulation time required to perform an optimization [Rizz04] which are summarized below:

- Space mapping
- Domain Partitioning
- Neural Network Modeling

Space mapping, first introduced by Bandler [Band94] [Band95] [Band03] [Bakr99], maps modestly accurate circuit models to very accurate EM simulation. In doing so, optimization can be performed in the circuit model space and layout derived by inverting the map. Simulation times are reduced since only the minimum number or expensive EM simulations are performed.

Domain Partitioning is a technique in which a network is divided into smaller sub-networks [Howa91] [Band97] [Bila97] [Sonnet]. EM analysis can then be performed on each partition of the network individually. This naturally leads to faster simulation times. One important limitation of this approach is that a given sub-network must exhibit very little coupling with any other sub-network.

Neural Networks follows naturally on the Domain Partitioning technique. Whereas a Partition would need to be simulated inside the optimization loop, all EM analysis could be performed prior to the optimization and then modeled using a neural network [Rizz04] [Zaab95]. The advantage is that statistical analysis techniques can be employed even though they require an abundance of data. Regarding EM coupling, this technique has the same limitation as the Domain Partitioning technique.

The proposed approach takes the advantages of the domain partitioning technique, but also retains accuracy of fine simulation data by including the effects of coupling. The proposed approach only makes use of fine EM simulation data.

In terms of simulation speed, the proposed method can have a significant advantage over other methods that also make use of EM simulations. This results from the fact that a full range of data can be obtained with fewer and smaller simulations by using coupling models. This is essential when an optimization is run that requires random starting points such as in [Band95].

The following example demonstrates this with an example of optimization in which the process can be improved by using coupling models. In figure 3-11 shown below, the cascade circuit is composed of 4 components. Each component can be optimized by choosing one of five possible component values. Thus there are 625 possible complete circuits. Without using coupling components, 625 large simulations (i.e., involving more than two components) must be performed.

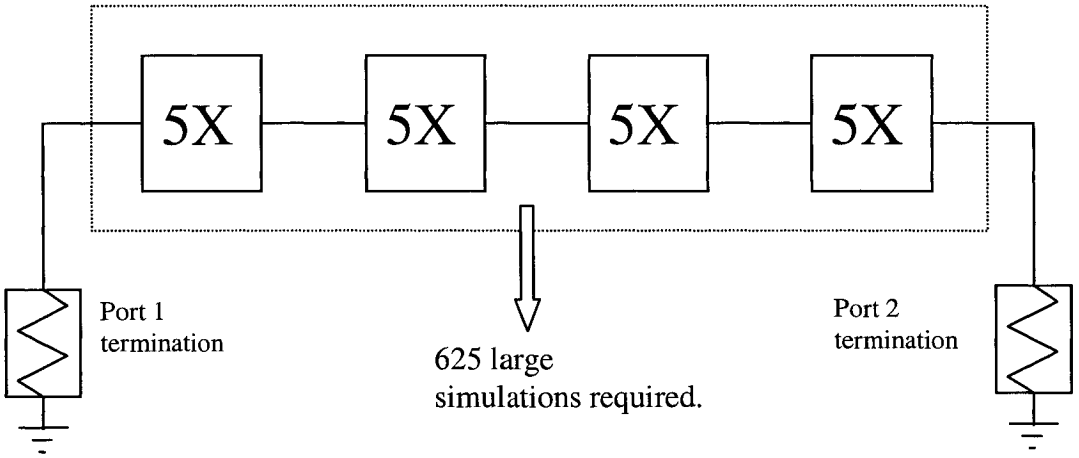

Figure 3-11. Four element circuit to be optimized. Each component can be optimized using one of 5 (5X) component values.

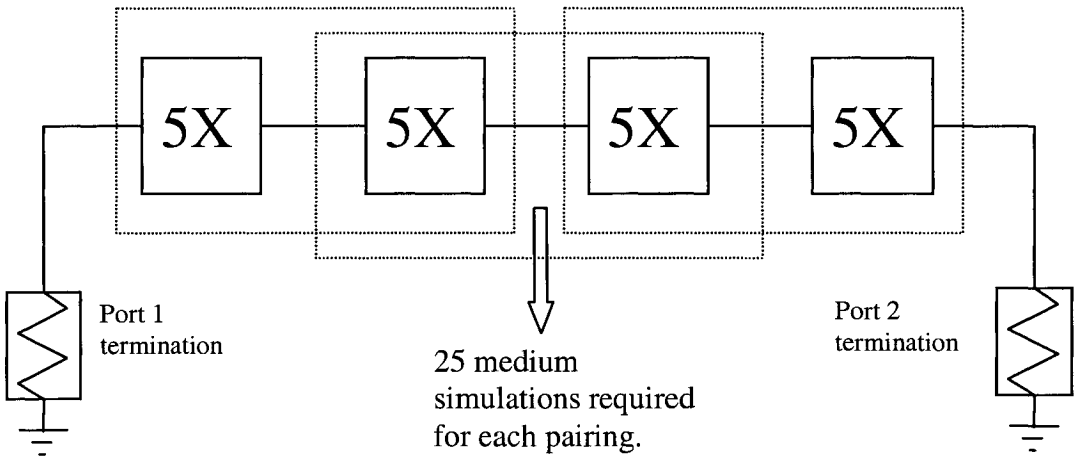

Figure 3-12. Four element circuit to be optimized using Coupling components.

Simulation of the identical circuit using coupling models with the same amount of possible component values is shown in figure 3-12. Without taking coupling into account, small (1 component) simulations can be performed to achieve results for every combination in only 20 small simulations [Sonnet]. However, the error has been shown to be non-negligible at high

frequency [Yago04]. To include coupling, 25 simulations are required for each pairing along with the 5 small simulations for each component. The resulting total amount of simulations using coupling components are 75 medium simulations and 20 small simulations.

The advantage of using coupling components in this fashion becomes more and more apparent with more complex circuits.

Table 3-2. Number of Small (1component), Medium (2 component) and large (all components) simulations required in the discrete optimization process of a band pass filter.

Components	Using Coupling Components: 5 possibilities per component			Using Single Simulations: 5 possibilities per component		
	Small Sims.	Medium Sims.	Large Sims.	Small Sims.	Medium Sims.	Large Sims.
2	10	25	0	0	25	0
3	15	50	0	0	0	125
4	20	75	0	0	0	625
5	25	100	0	0	0	3125
10	50	225	0	0	0	$9*10^6$
20	100	475	0	0	0	$95*10^{12}$

As shown in table 3-2, using coupling components can reduce the size and number of simulations needed to optimize a circuit while maintaining accuracy. The time needed to simulate is reduced not only because smaller less complex simulations are achieved relatively faster [Sonnet] but also because the number of simulations increases linearly with the addition of new components rather than exponentially.

3.6.1 Optimization Comparison with EM Tools

Sonnet has introduced Optimization tools very similar to the approach mentioned above. It allows the circuit to be subdivided into smaller pieces which greatly reduces the matrix solve time. According to [Sonnet], the matrix solve time is directly proportional to the cube of the number of subsections. Thus if a circuit is divided in half, the matrix solve time will be four times faster. If a large circuit is subdivided into 3 smaller subsections, the simulation could be performed 14 times faster [Sonnet]. However, we have found that reference planes are necessary to eliminate effects of coupling to remove port discontinuities and effects from the metal box wall. As such there is some overhead in subdividing the circuit and is considered a limitation to sonnet *em*'s approach.

Also according to [Sonnet], inaccuracies can be introduced specifically due to coupling. Therefore, circuit subdivisions have to be selected where coupling is not significant.

The research presented in this thesis represents a step forward in this important area. At the cost of performing more simulations, the accuracy is increased by using coupling models over other methods that also subdivide the network by including the effects of coupling.

3.7 Conclusion

In this chapter, we have presented a new and efficient method for coupling computation in microwave structure design. Methods for modeling coupling in Series, Parallel and Arbitrarily

connected networks have been demonstrated. The limitations of the proposed approach have also been carefully considered and weighed against benefits. It was shown that coupling models can be extremely useful in simulation and designs using lumped components at high frequencies where coupling is present. While maintaining accuracy, coupling models can save on expensive simulation time in applications like discrete optimization.

3.8 References

[Bakr99] M. Bakr, J. Bandler, N. Georgieva, K. Madsen, "A hybrid aggressive space-mapping algorithm for EM optimization," *IEEE Trans. On Microwave Theory and Tech.*,1999, 2440 – 2449.

[Band94] J.Bandler, R.Biernacki, S.Chen; P.Grobelny, R.Hemmers, "Space mapping technique for electromagnetic optimization," *IEEE Trans. On Microwave Theory and Tech.*,1994, 2536 - 2544.

[Band95] J. Bandler, R. Biernacki, S. Chen, R. Hemmers, K. Madsen, "Electromagnetic optimization exploiting aggressive space mapping," *IEEE Trans. On Microwave Theory and Tech.*,1995, 2874 - 2882.

[Band97] J. Bandler, R. Biernacki, S. Chen, Y. Huang;, "Design optimization of interdigital filters using aggressive space mapping and decomposition," *IEEE Trans. On Microwave Theory and Tech.*, 1997, 761 – 769.

[Band03] J. Bandler, Q. Cheng, S. Dakroury, A. Mohamed, M. Bakr, K. Madsen, J. Sondergaard, "Space mapping: the state of the art [circuit simulation, CAD]," *IEEE Int. Microwave and Optoelectronics Conf.*, 2003, 951 – 956.

[Baud97] H. Baudrand, "Electromagnetic study of coupling between active and passive circuits", *IEEE Int. Microwave and Optoelectronics Conf.,* 1997, 143-152.

[Bila97] S. Bila, D. Baillargeat, S. Verdeyme, P. Guillon, "Automated electromagnetic optimization method for microwave devices," *IEEE Microwave and Guided Wave Letters*,1997, 242 – 244.

[Chen01] C. Chen and M. Deen, "A general noise and s-parameter deembedding procedure for on-wafer high-frequency noise measurements of MOSFETs," *IEEE Trans. On Microwave Theory Tech.*, 2001, 1004-1005.

[Fric94] D.A. Frickey, "Conversions between S, Z, Y, h, ABCD, and T parameters which are valid for complex source and load impedances," *IEEE Trans. On Microwave Theory Tech.*, 1994, 205-211.

[Frid98] D. Friday, "Microwave technology: directions and measurement requirements for the 21th century", *Microwave J.*, 1998, 110-114.

[Gupt81] K.C. Gupta, R. Garg, R. Chadha, *Computer aided design of microwave circuits*, Artech House, Dedham (1981).

[Howa91] G. Howard, Y. Chow, "A high level compiler for the electromagnetic modeling of complex circuits by geometrical partitioning," *IEEE Microwave Symposium Digest*, 1991, 1095 – 1098.

[Maple] *Maple V reference manual*, New-York.

[Mona74] V. Monaco, P. Tiberio, "Computer-Aided Analysis of Microwave Circuits," *IEEE Trans. On Microwave Theory Tech.*,1974, 249-263.

[Rizz04] V. Rizzoli, A. Costanzo, D. Masotti, A. Lipparini, F. Mastri, "Computer-aided optimization of nonlinear microwave circuits with the aid of electromagnetic simulation," *IEEE Trans. On Microwave Theory and Tech.*, 2004, 362 – 377.

[Sonnet] Sonnet User's Manual, Vol.1, Release 7.0, Sonnet Software Inc., Liverpool, NY.

[Yago04] M.C.E. Yagoub, P. Sharma, "Characterization of EM effects in RF/microwave integrated circuits," *34th European Microwave Conf.,* 2004, Amsterdam, Netherlands, 221-224.

[Yin03] W.Y. Yin, S.J. Pan, L.W. Li, Y.B. Gan, "Experimental characterization of coupling effects between two on-chip neighboring square inductors", *IEEE Trans. On Electromagnetic Compatibility*, 2003, 557-561.

[Zaab95] A. Zaabab, Q. Zhang, M. Nakhla, "A neural network modeling approach to circuit optimization and statistical design," *IEEE Trans. On Microwave Theory and Tech.*, 1995, 1349 – 1358.

CHAPTER IV
RESULTS

To demonstrate the accuracy of our approach, different circuit configurations were considered, namely Series Connected Circuits (section 4.1), Parallel Connected Circuits (section 4.2) and lastly Arbitrarily Connected Circuits (section 4.3). Finally, our coupling models were used to optimize a band pass filter (section 4.4).

Before conducting any demonstrations of the coupling models, it was necessary to find the appropriate length of reference planes required to eliminate any interference or undesired coupling from the box wall. As stated in section 3.5, coupling to the box wall will introduce error into our analysis. The length of the reference plane was swept to arrive to the optimal value. A simple Resistor-Inductor-Capacitor (RLC) circuit was considered as shown in figure 4-1.

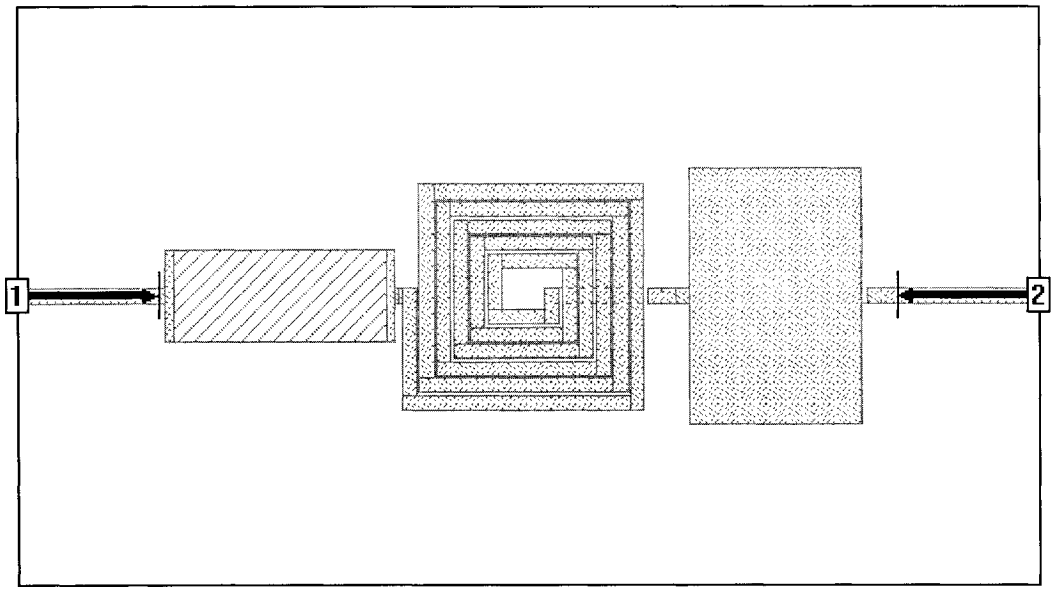

(a)

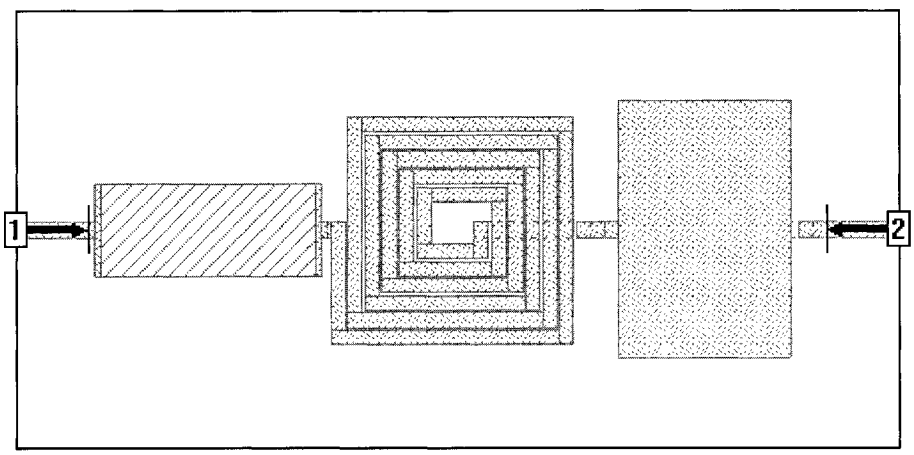

(b)

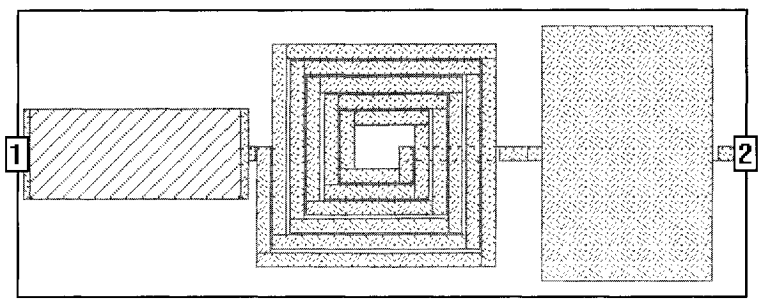

(c)

Figure 4-1. Series RLC Circuit used to determine optimal reference plane lengths. Reference plane lengths of 100μm (a), 50μm (b) and 0μm (c) are considered.

Simulation results are shown in figure 4-2. Resulting from an analysis of the simulation data, a reference plane length of 50μm was chosen for all simulations. Simulations using a reference plane of 100μm represent the most accurate data, however the simulations required too much time and memory size to be practical whereas 50μm reference plane simulations yield faster simulations with high accuracy.

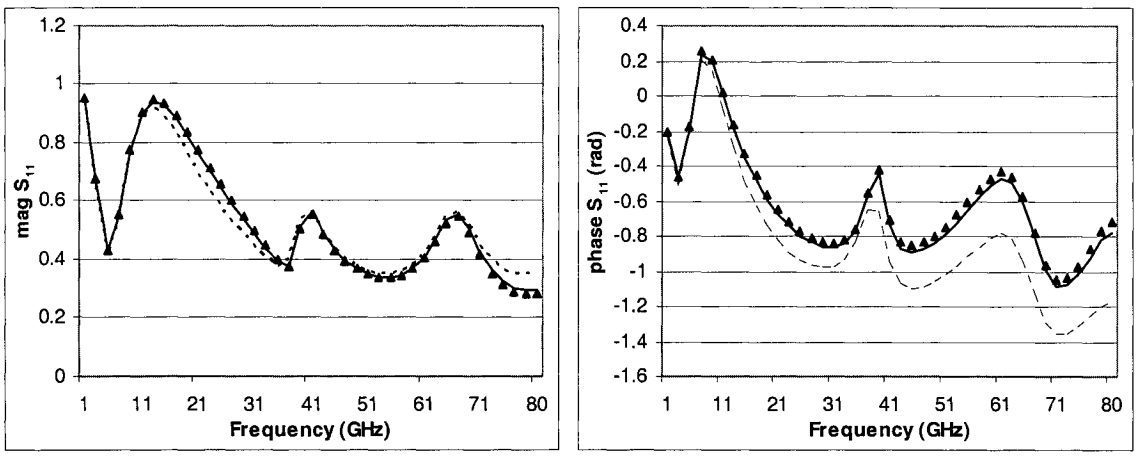

(a)

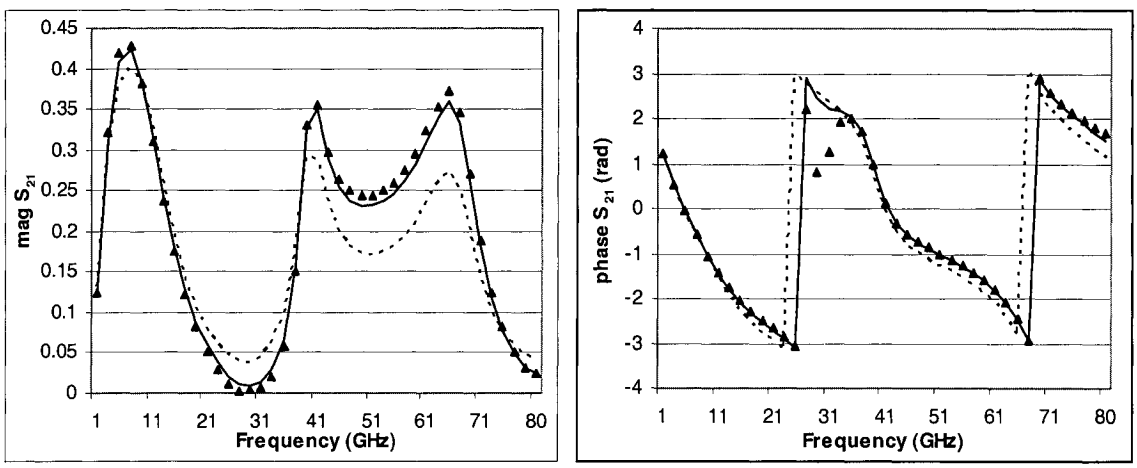

(b)

Figure 4-2. RLC circuit: Comparison of S_{11} (a) and S_{21} (b) magnitude and phase response obtained by using 100μm reference plane (▲) with those simulated using 50μm reference plane (—) and no reference plane (--). The reference planes are shown in Fig. 4-1

4.1 Evaluation Of Coupling In Series Connected Networks

4.1.1 Series Resistor Inductor Capacitor Circuit

The results for a series Resistor Inductor Capacitor (RLC) circuit are shown in figures 4-3 to 4-5. The results verify that coupling components can accurately model the electromagnetic coupling in series configurations. In fact, both magnitude and phase measurements are much more accurate over other results that do not include the coupling.

The cascaded Resistor- Inductor-Capacitor network that was simulated is shown in figure 4-1b. The EM simulator used is Sonnet *em*[Sonnet]. The circuit is built on 120μm GaAs substrate (ε_r = 12.9). The resistor is made from a 40 Ohm/Square material, and measures 150 μm x 65 μm. The inductor has 5.5 turns with a line width of 10 μm, line spacing of 2 μm, and an inside square length of 30 μm. By examining the results, it is apparent that the circuit has several self resonant frequencies. The capacitor has an area of 120 μm x 180 μm where the distance between the plates is 1 μm.

The coupling components were simple to calculate and the results are in close agreement with those simulated from EM simulation.

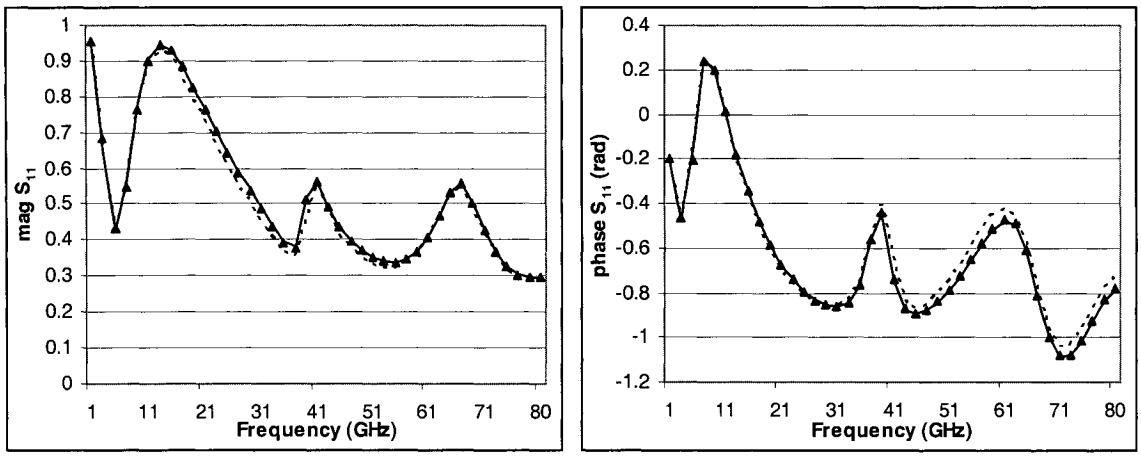

Figure 4-3. RLC circuit: Comparison of S_{11} magnitude and angle obtained by using coupling components (—) with those simulated in Sonnet (▲) and assuming no coupling (- -).

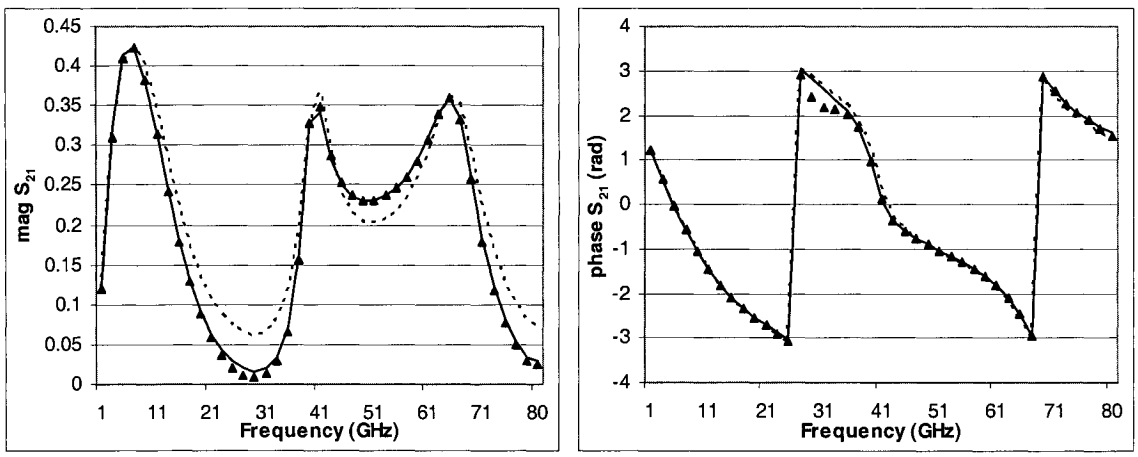

Figure 4-4. RLC circuit: Comparison of S_{21} magnitude and angle obtained by using coupling components (—) with those simulated in Sonnet (▲) and assuming no coupling (- -).

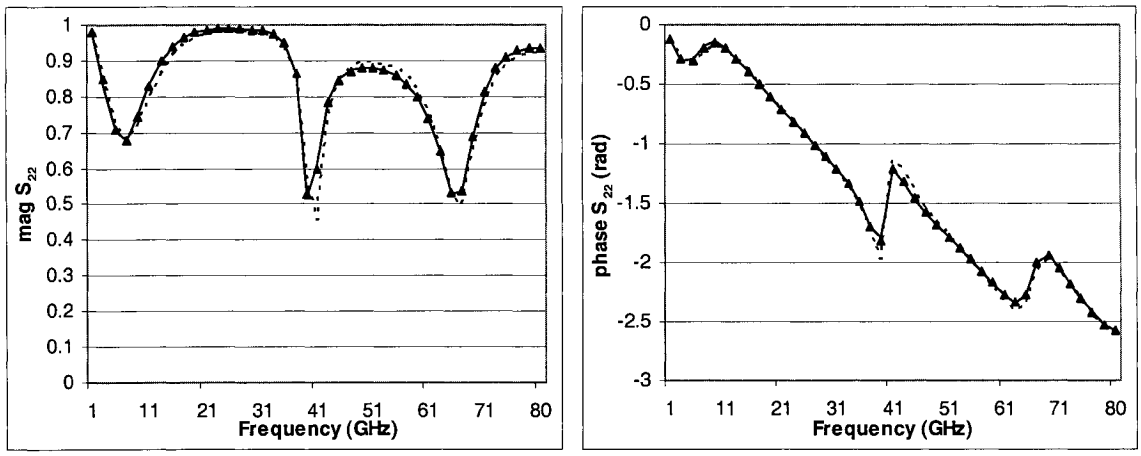

Figure 4-5. RLC circuit: Comparison of S_{22} magnitude and angle obtained by using coupling components (—) with those simulated in Sonnet (▲) and assuming no coupling (- -).

4.1.2 Chebyshev Lowpass Filter

To examine the effect of coupling in a more practical circuit, a lowpass chebyshev filter was designed using the following specifications:

$f_c = 12.5GHz$ *filter cutoff frequency*
$A_m = 0.5dB$ *passband ripple magnitude*
Minimum rejection at $f_c + 3GHz = 20dB$

Using the design equations given in Appendix III, the filter was realized as follows:

$L_1 = 0.78$ nH
$C_1 = 0.377$ pF
$L_2 = 1.39$ nH
$C_2 = 0.417$ pF
$L_3 = 1.39$ nH
$C_3 = 0.377$ pF
$L_4 = 0.78$ nH

Agilent *Advanced Design System* (*ADS*) [ADS] was used for initial simulation and optimization of the filter which is shown here in Figure 4-6:

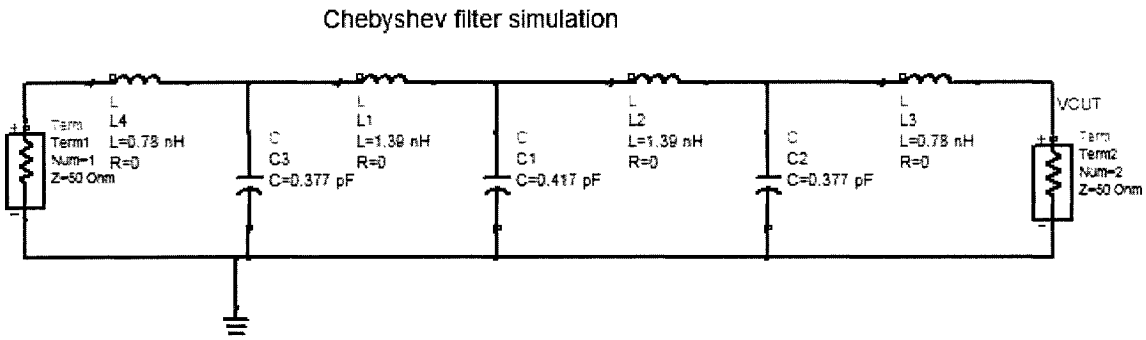

Figure 4-6. Lowpass Chebyshev Filter circuit in *ADS*.

To verify the initial design, the circuit was simulated using *ADS*.

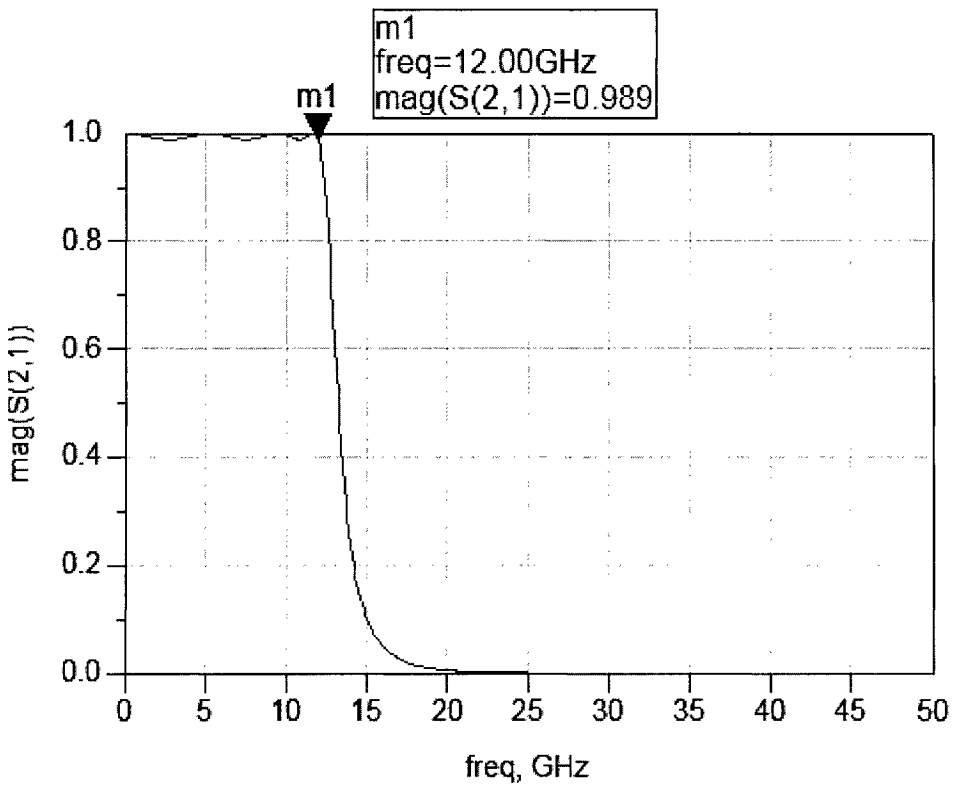

Figure 4-7. Simulated forward transmission response (S_{21}) of the lowpass filter in *ADS*.

Due to parasitic and fringing field capacitance, the capacitance value for a given capacitor varies with frequency. Similarly, for inductors the inductance value tends to vary especially when close to the Self Resonant Frequency (SRF). Knowing that this effect would distort the expected response of the entire circuit, the capacitive and inductive components were carefully chosen to have correct values at the cutoff frequency.

Table 4-1. Low pass filter component values.

Component	Geometrical Parameter
$L_1 = L_4$	n= 2.5 turns, il = 45μm, w = 10μm, s = 2μm
$L_2 = L_3$	N = 3.5 turns, il = 40 μm, w = 10 μm, s = 2 μm
$C_1 = C_3$	L = 160 μm, W = 260 μm
C_2	L = 160 μm, W = 244 μm

For the inductors, geometrical parameter 'n' is the number of turns, 'il' is the inside spacing, 'w' is the line width and 's' is the distance between the metal lines. For the capacitor 'L' is the length and 'W' is the width of the capacitor plate.

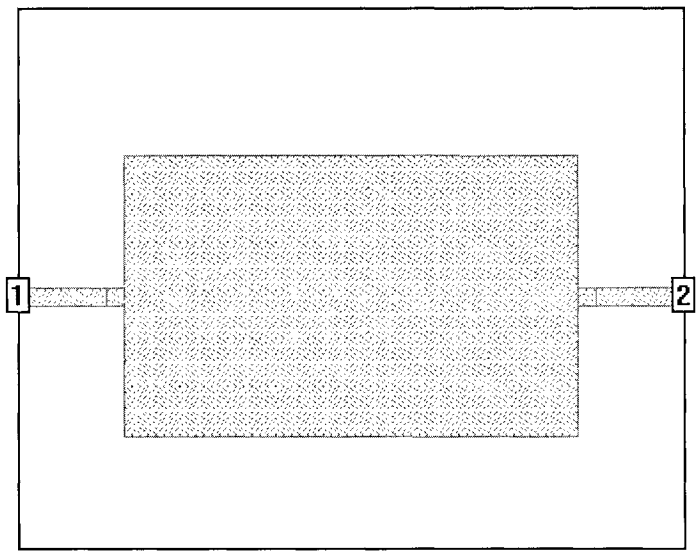

Figure 4-8. Capacitor used in the Chebyshev Lowpass filter.

Capacitor C_1 layout in Sonnet *em* is shown in figure 4-8. The reference plane in this simulation has been set to 50μm to remove any effects from the proximity of the box wall and effects from the transmission lines at the input and output. The top plate of the capacitor is shown. The bottom plate is connected to ground.

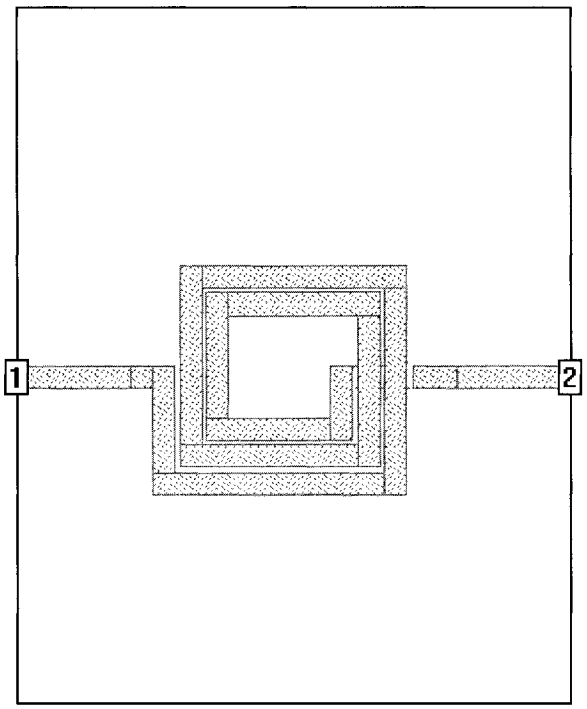

Figure 4-9. Inductor used in the Chebyshev Lowpass filter as shown in Sonnet *em*.

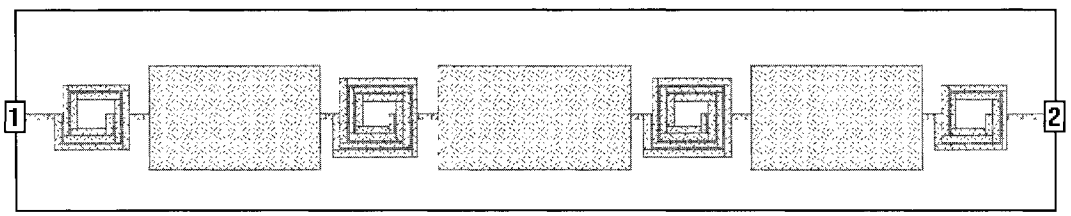

Figure 4-10. Lowpass Chebyshev filter layout in Sonnet *em*.

Using formulas derived for calculating series coupling components, the coupling is calculated for each pair of components. Equation 4.1 represents the overall circuit response using the coupling components while 4.2 represents the overall circuit response without coupling:

$$T\,coupling = T_{L1} * T^{X}_{L1C1} * T_{C1} * T^{X}_{C1L2} * T_{L2} * T^{X}_{L2C2} * T_{C2} * T^{X}_{C2L3} * T_{L3} * T^{X}_{L3C3} * T_{C3} * T^{X}_{C3L4} * T_{L4} \quad (4.1)$$

where T_L, T_C, T_{LC} and T_{CL} are the T-matrix's for an inductor, capacitor, and coupling models for the inductor-capacitor and capacitor-inductor respectively.

$$T\,no\,coupling = T_{L1} * T_{C1} * T_{L2} * T_{C2} * T_{L3} * T_{C3} * T_{L4} \quad (4.2)$$

The results in figures 4-11 to 4-13 show that including coupling components improves simulation accuracy at frequencies above 45GHz, where the effects of coupling become very significant.

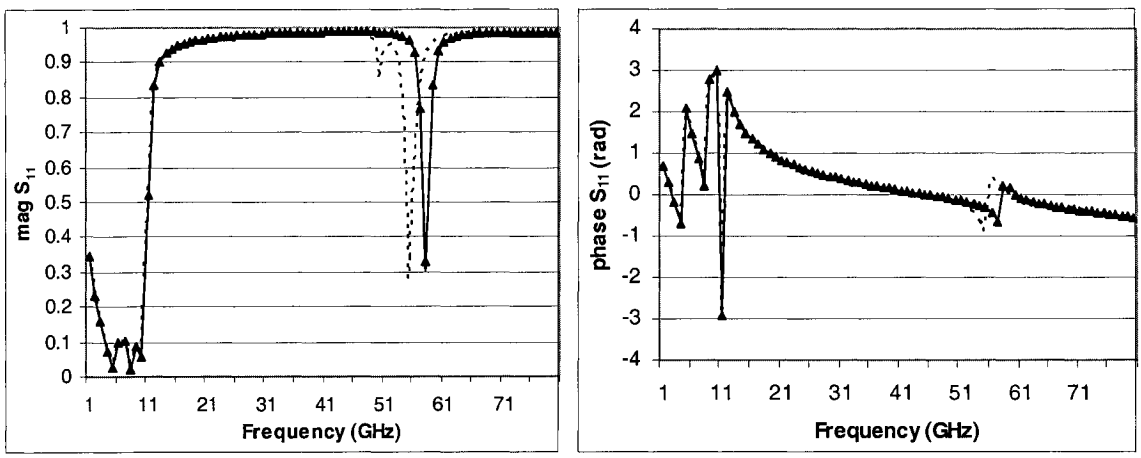

Figure 4-11. Chebyshev lowpass circuit: Comparison of S_{11} magnitude and angle obtained by using coupling models (—) with those simulated in Sonnet (▲) and assuming no coupling (- -).

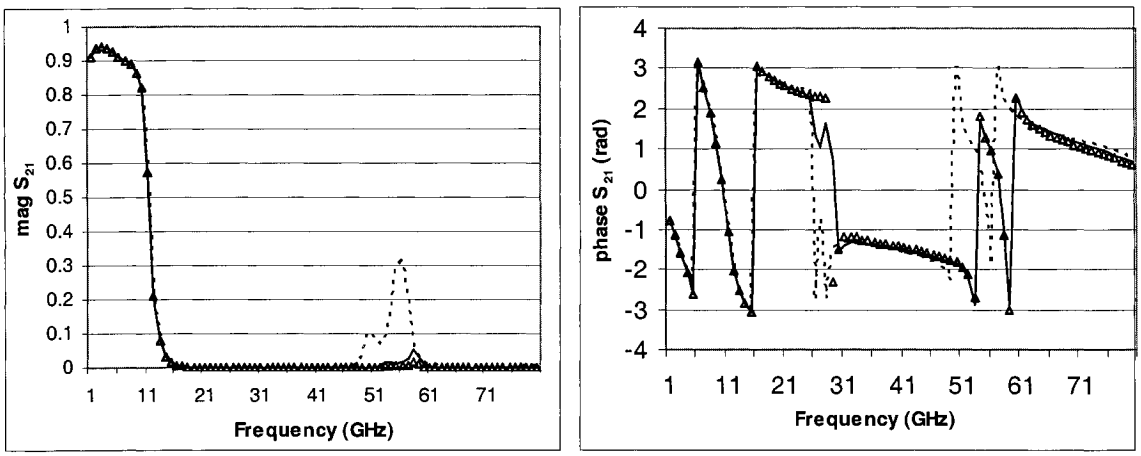

Figure 4-12. Chebyshev lowpass circuit: Comparison of S_{21} magnitude and angle obtained by using coupling models (—) with those simulated in Sonnet (▲) and assuming no coupling (- -).

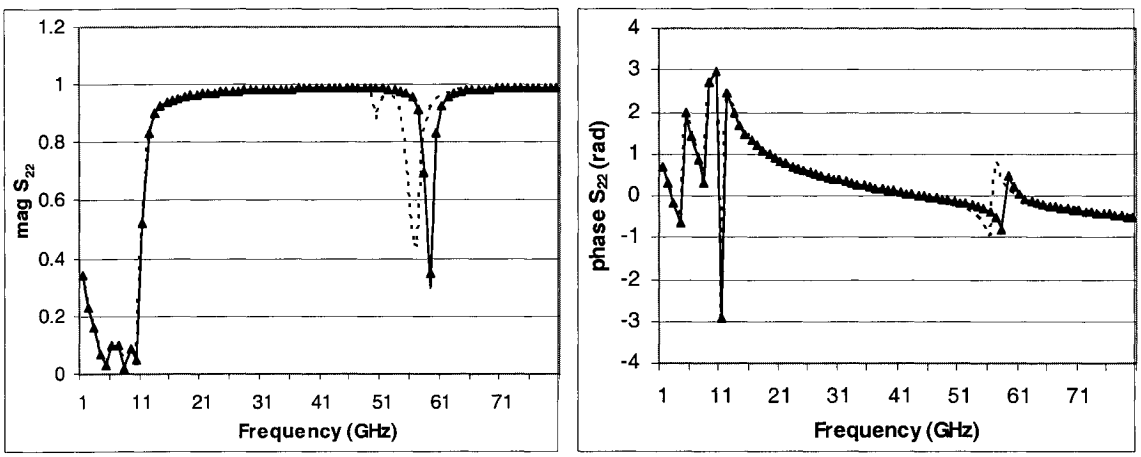

Figure 4-13. Chebyshev lowpass circuit: Comparison of S_{22} magnitude and angle obtained by using coupling models (—) with those simulated in Sonnet (▲) and assuming no coupling (- -).

4.2 Evaluation Of Coupling In Parallel Connected Networks

A parallel representation of a RLC network was constructed to demonstrate the accuracy of our coupling models in parallel networks. To increase the coupling effects, we put the inductor between the resistor and the capacitor and reduced all interconnect lengths.

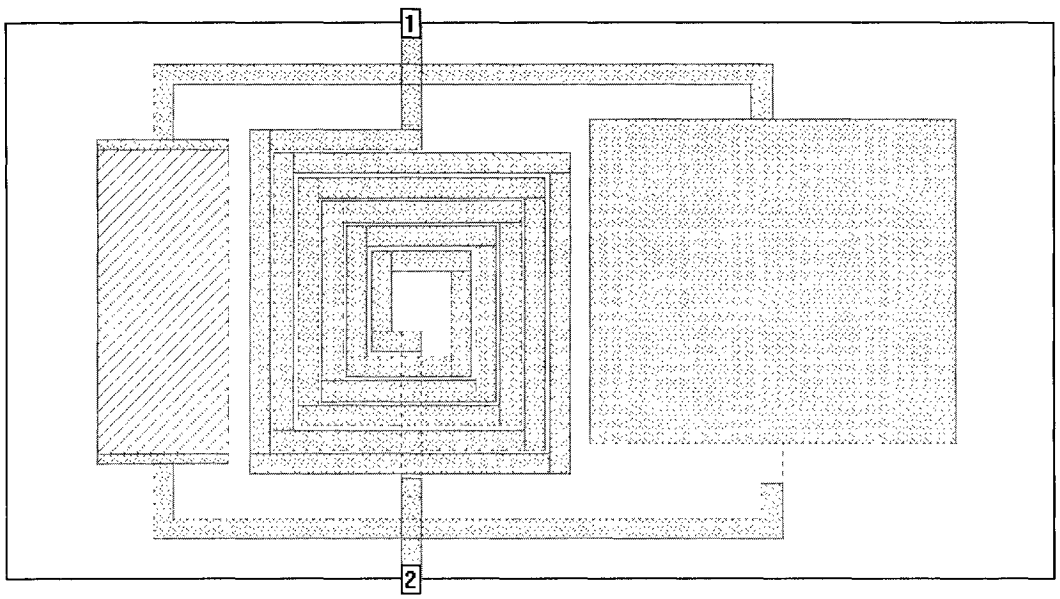

Figure 4-14. Parallel RLC circuit.

The results using coupling components were computed using individual Y-parameters of each component along with coupling components (one between the resistor and inductor, and another between the inductor and capacitor). The expected results are from a single simulation of the completed circuit. As expected, the results generated from the coupling component show excellent agreement with expected results from Sonnet *em*.

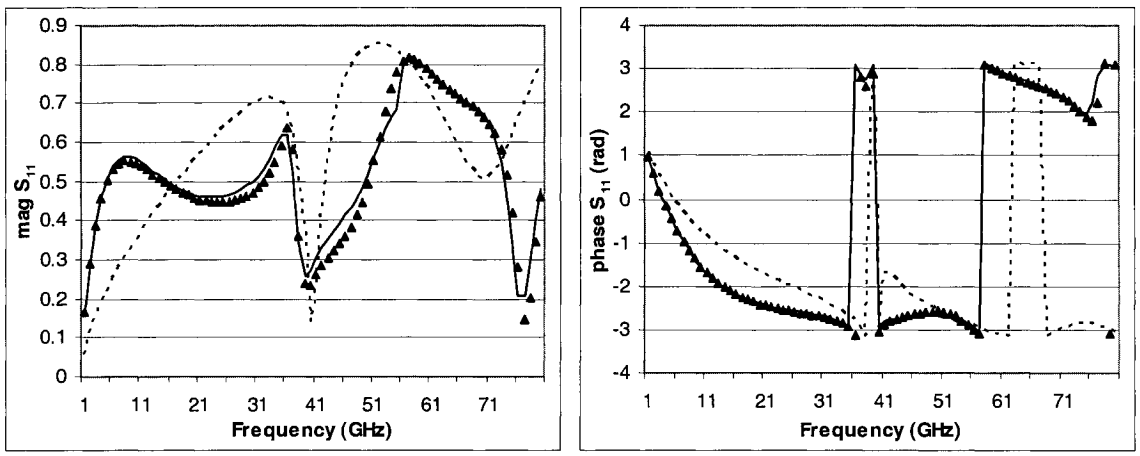

Figure 4-15. Parallel RLC circuit: Comparison of S_{11} magnitude and angle obtained by using coupling models (—) with those simulated in Sonnet (▲) and assuming no coupling (- -).

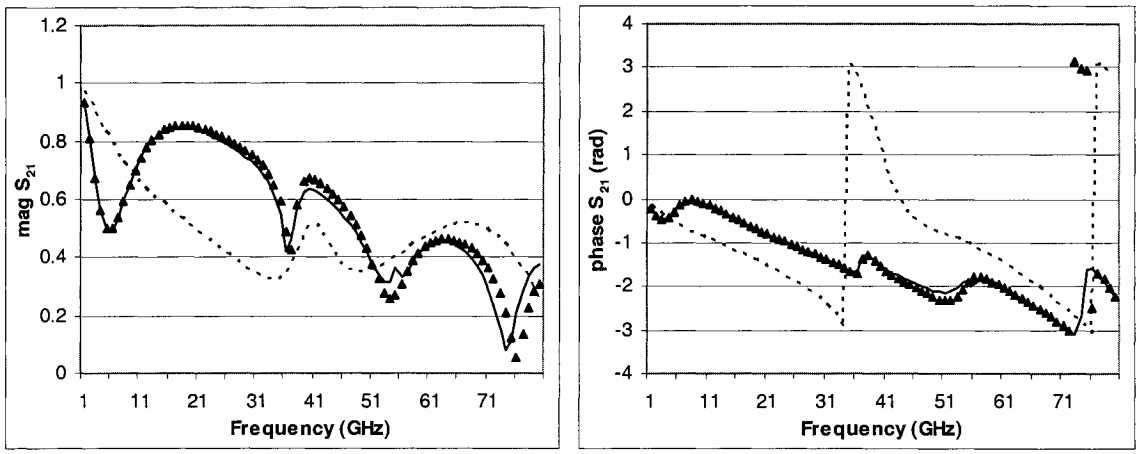

Figure 4-16. Parallel RLC circuit: Comparison of S_{21} magnitude and angle obtained by using coupling models (—) with those simulated in Sonnet (▲) and assuming no coupling (- -).

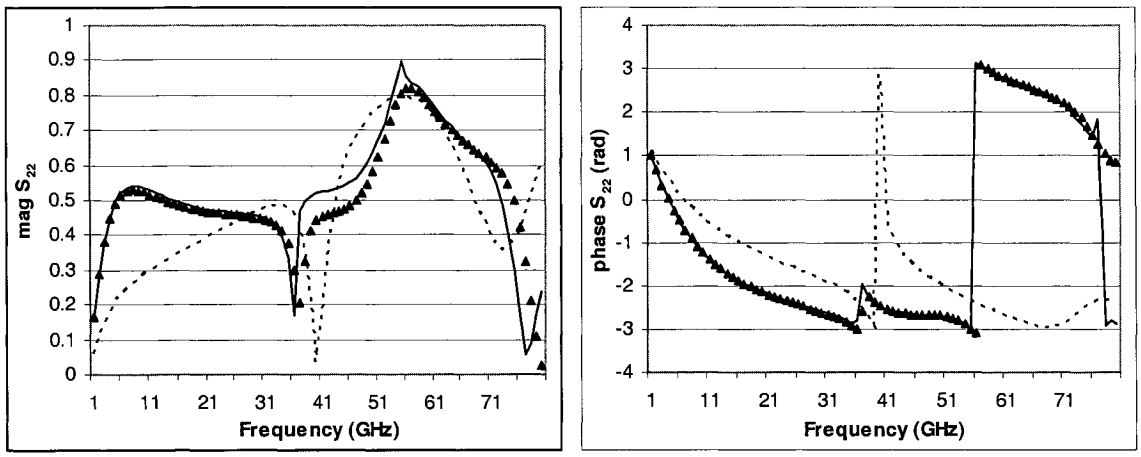

Figure 4-17. Parallel RLC circuit: Comparison of S_{22} magnitude and angle obtained by using coupling models (—) with those simulated in Sonnet (▲) and assuming no coupling (- -).

4.3 Evaluation Of Coupling In Arbitrarily Connected Networks

For any arbitrarily connected circuit, the Connection Scattering Matrix method can be used to derive equations for coupling models. This section presents results using the Connection Scattering Matrix method first for obtaining coupling models in a T-junction circuit and then in an output matching circuit.

4.3.1 T-junction Coupling

The method used to de-embed the intrinsic transistor and then the buffer circuit was applied also for coupling. We begin with a simple capacitive circuit shown in figure 4-18 which was simulated using Sonnet *em*[Sonnet]. Our code was then used to extract the coupling and compare to the same circuit response assuming no coupling.

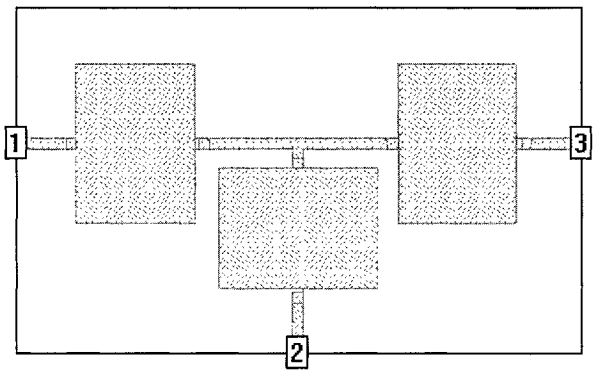

Figure 4-18. Capacitive T-junction circuit.

The circuit layout is from Sonnet *em*[Sonnet]. All capacitors are 120μm by 160μm on 50μm GaAs substrate (ε_r = 12.9). At 10GHz, each individual capacitor exhibits 0.137pF capacitance.

As shown in below, the de-embedded technique developed above for coupling allowed us to obtain very close results to the original data simulated in Sonnet *em*[Sonnet].

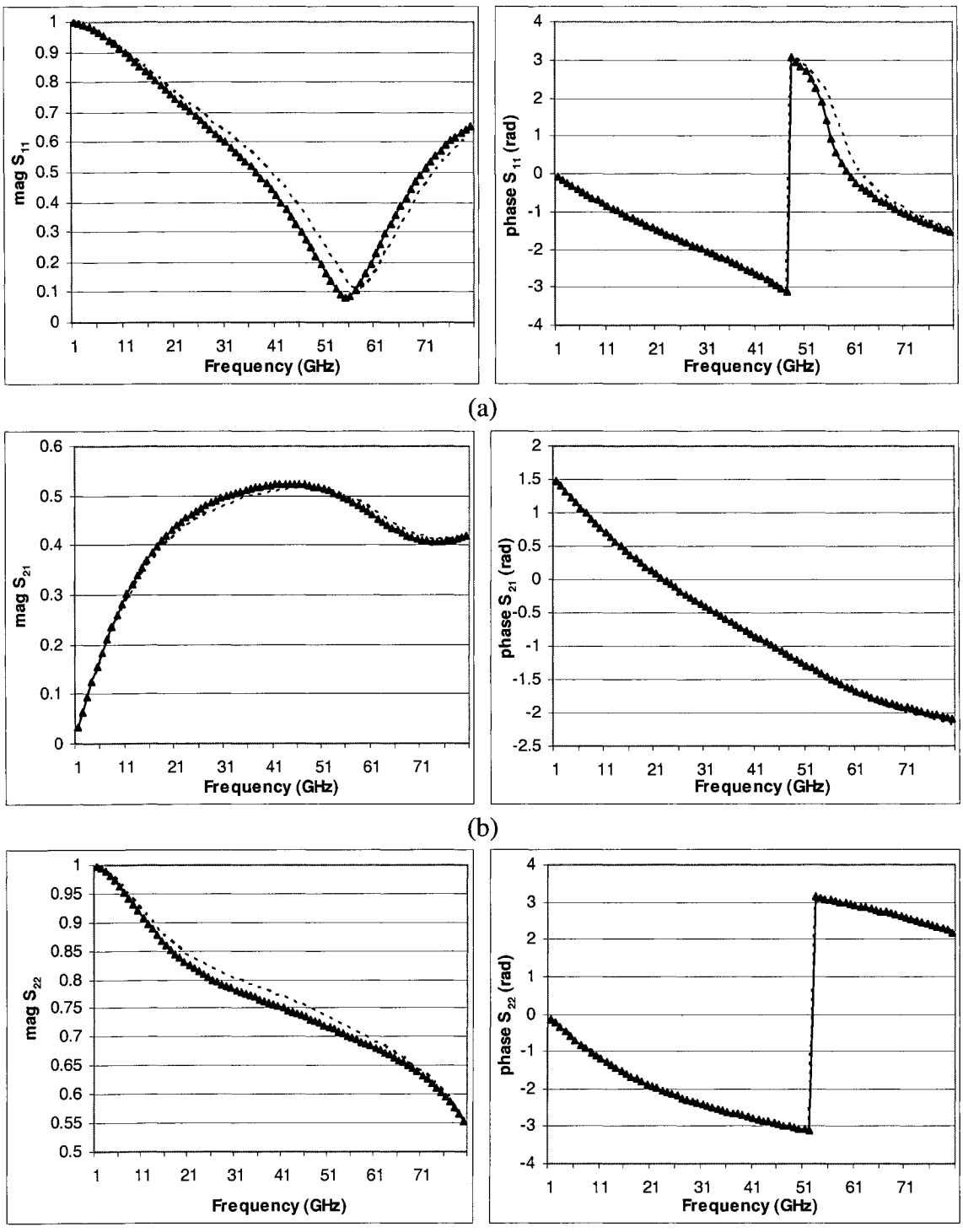

Figure 4-19. T Capacitive circuit: Comparison of S_{11} (a), S_{21} (b) and S_{22} (c) magnitude and angle obtained from using coupling models(—) with those simulated in Sonnet (▲) and assuming no coupling (- -).

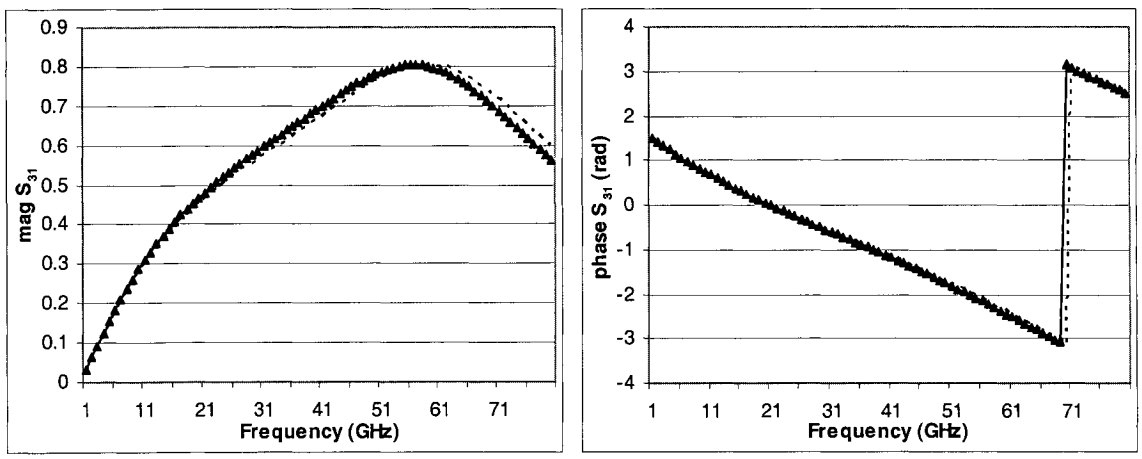

(a)

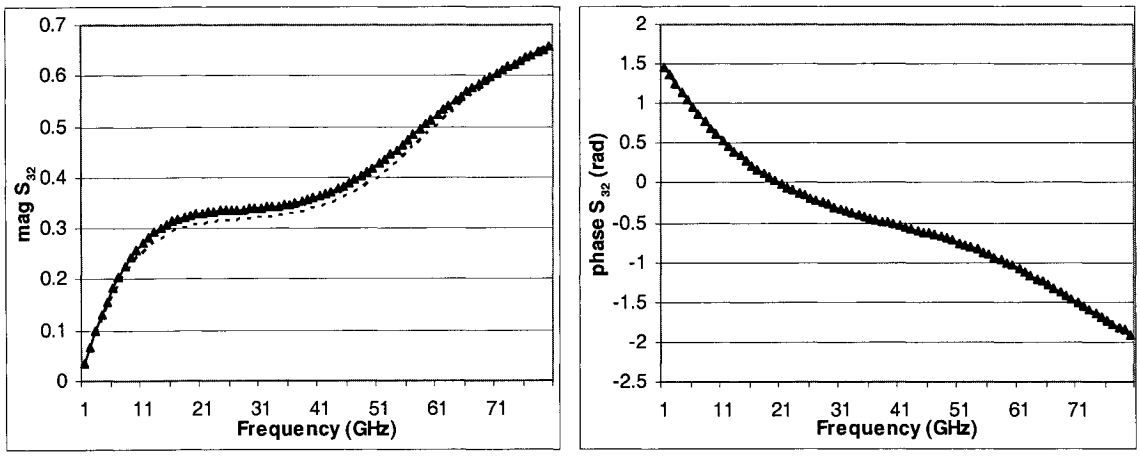

(b)

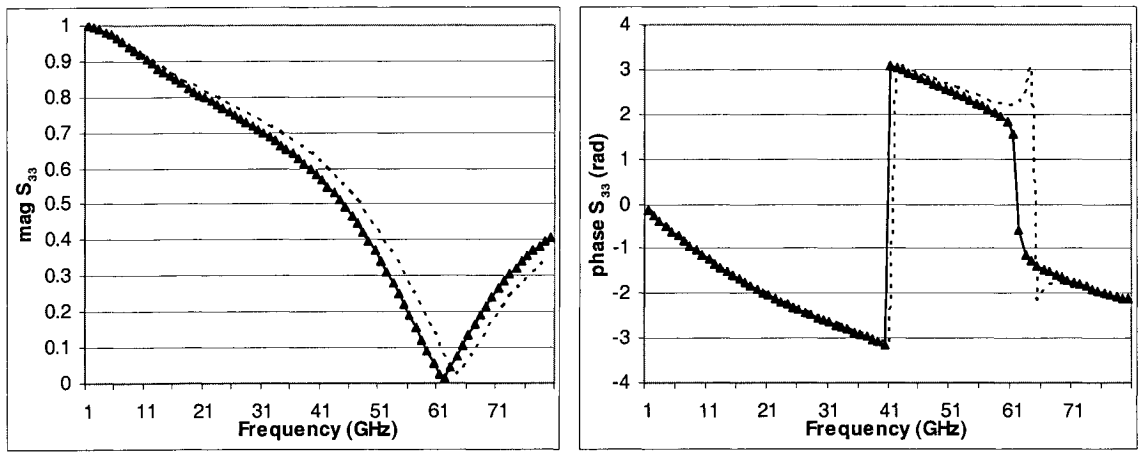

(c)

Figure 4-20. T Capacitive circuit: Comparison of S_{31} (a), S_{32} (b) and S_{33} (c) magnitude and angle obtained from using coupling models(—) with those simulated in Sonnet (▲) and assuming no coupling (- -).

4.3.2 Output Matching Circuit

The accuracy of our modeling technique for three port networks was demonstrated using the three port capacitive circuit. Next a more functional circuit was considered. This was an output matching circuit designed for an HBT transistor based amplifier. The output matching circuit is shown in figure 4-21. Using Agilent *ADS* [ADS] design templates, the optimum load to present to the transistor was found to be (61.8 + j 58.12) ohms.

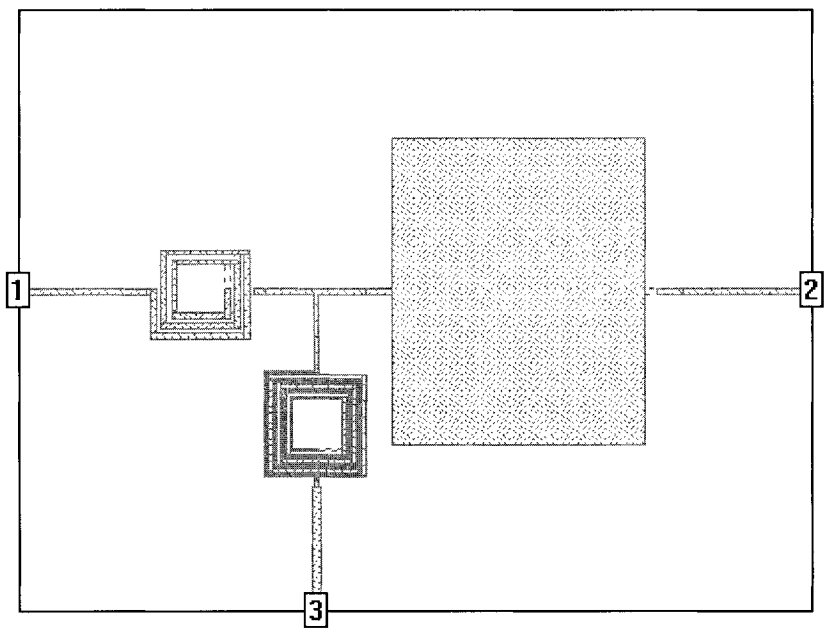

Figure 4-21. Output matching filter used for this example.

The output matching circuit had 50μm thick GaAs substrate. The circuit was comprised of the following components:

Series Inductor L_1 - There were 2.5 turns on the top metal and 2 turns on the bottom metal layers. Line thickness was 2μm, and line spacing was also 2μm. The inductor exhibits 1.4nH inductance at 20GHz with a Self Resonance (SRF) at close to 59GHz.

Shunt Inductor L_2 – This inductor is comprised of 5.5 turns on the top layer and 5 turns on the bottom layer. In order to increase the SRF, the line thickness was changed to 1μm with a 1μm spacing. This inductor had 9.44nH inductance at 20GHz with SRF close to 29GHz.

Series Capacitor – The Capacitor measures 100μm x 120μm and produced 0.12pF at 20GHz.

As shown from the results of this example, the connection scattering matrix technique for determining the coupling models is again shown to be accurate, this time using inductors as well as capacitors. The inductors in this particular application induce more significant coupling than in the tee connected capacitive circuit. Since we were using inductors at very high frequencies, special design considerations were taken into account in order to raise the inductor SRF frequencies past 25GHz. Methods to do this are outlined in Appendix IV.

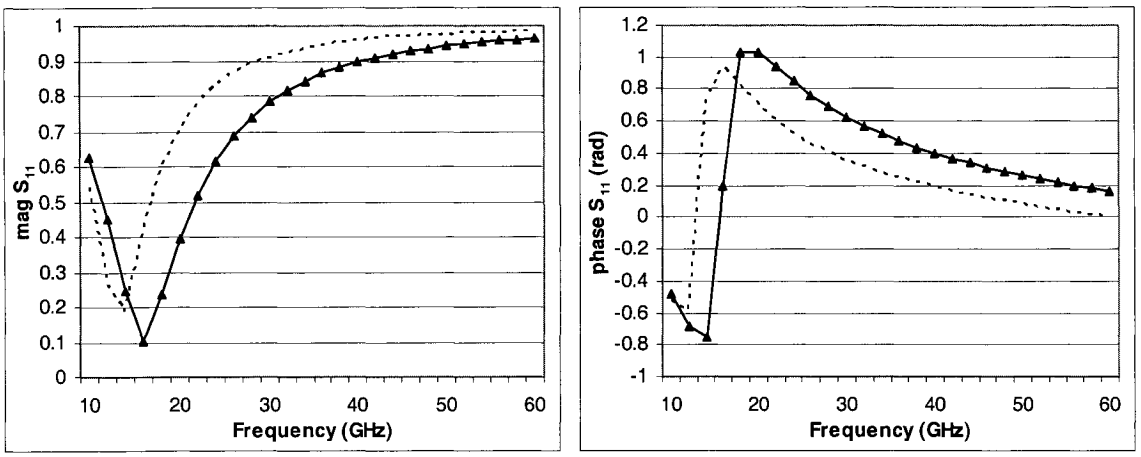

(a)

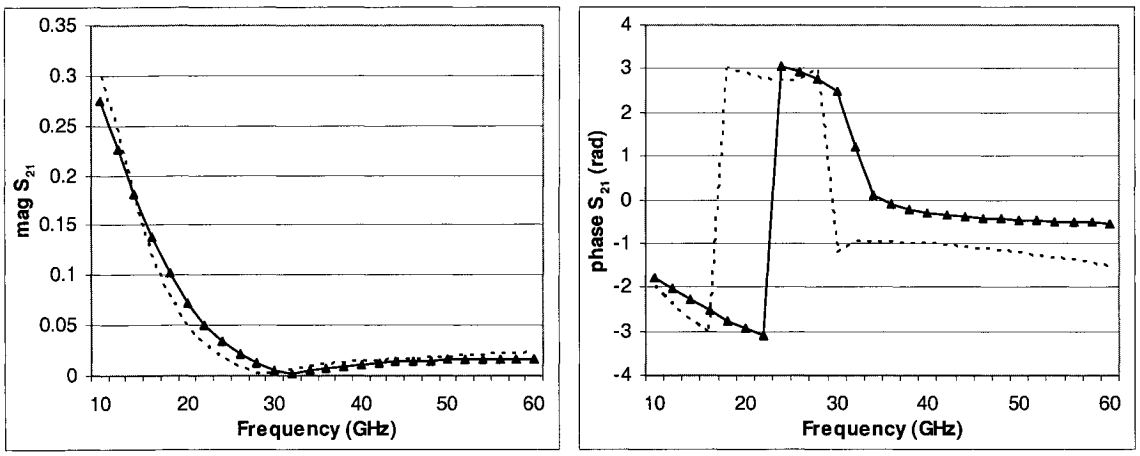

(b)

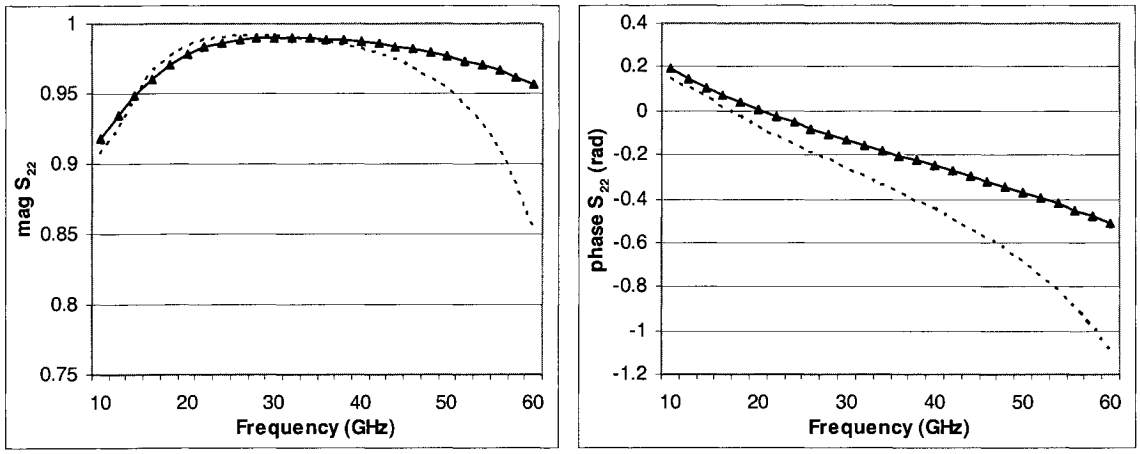

(c)

Figure 4-22. Output Matching circuit: Comparison of S_{11} (a), S_{21} (b) and S_{22} (c) magnitude and angle obtained from using coupling models(—) with those simulated in Sonnet (▲) and assuming no coupling (- -).

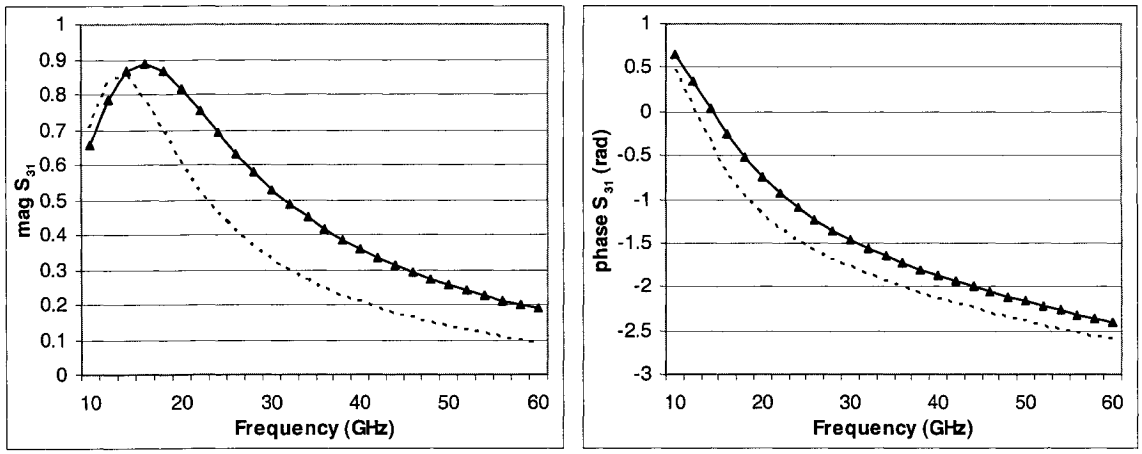

(a)

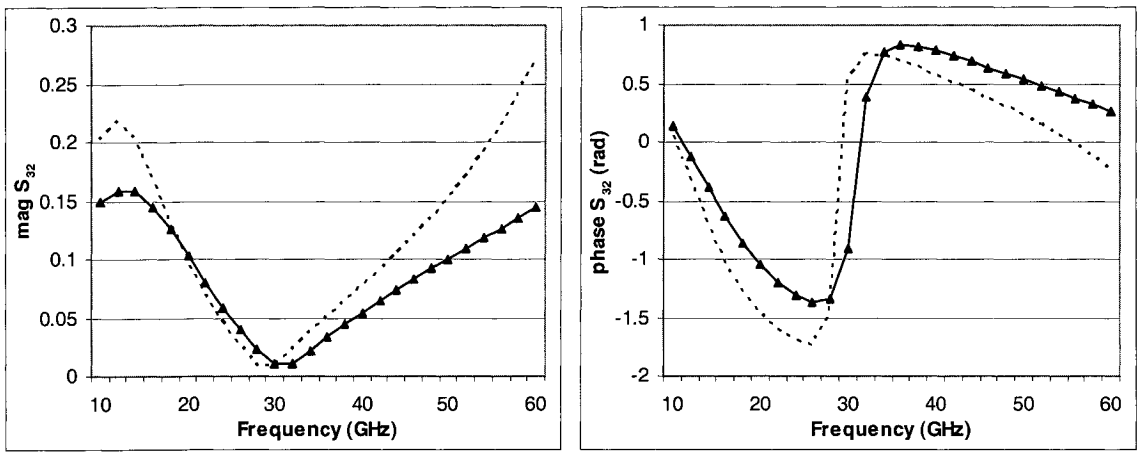

(b)

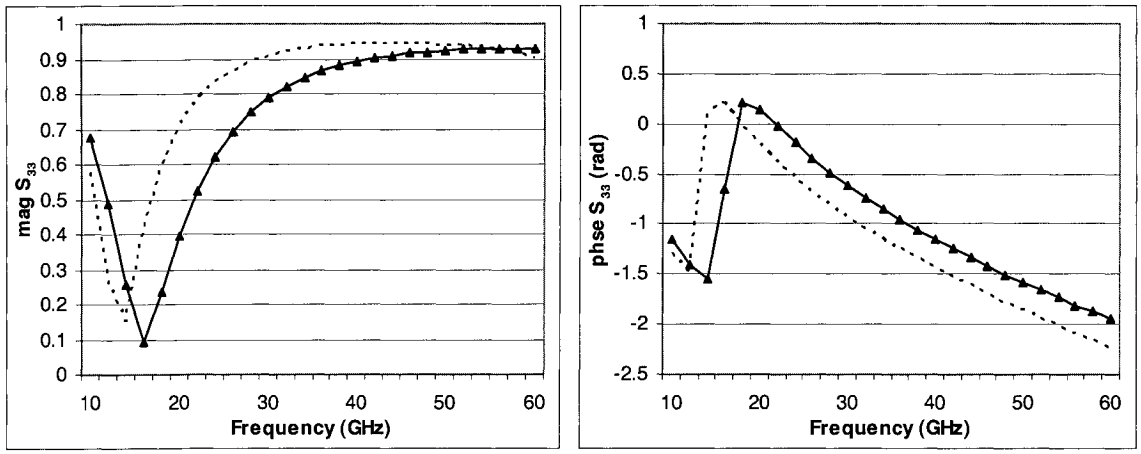

(c)

Figure 4-23. Output Matching circuit: Comparison of S_{31} (a), S_{32} (b) and S_{33} (c) magnitude and angle obtained from using coupling models(—) with those simulated in Sonnet (▲) and assuming no coupling (- -).

4.4 Optimization Using Coupling Models

A 2nd order band pass filter centered at 50 GHz is optimized for maximum S_{21} and minimum S_{11}. Figure 4-24 shows the resulting schematic from an optimization process from *ADS* [ADS].

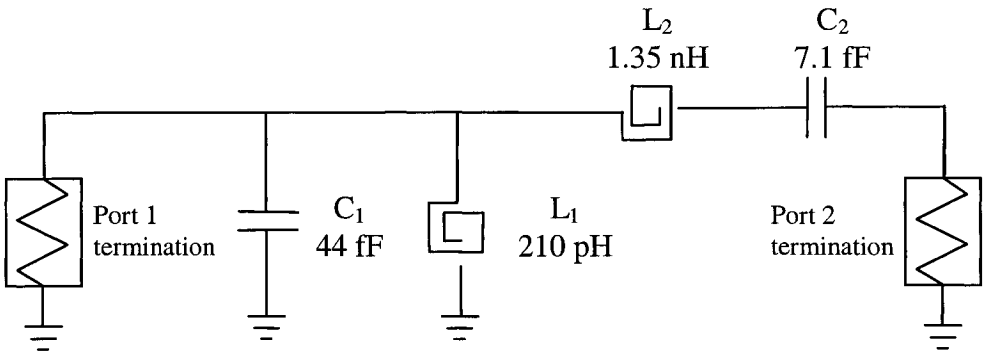

Figure 4-24. Band pass filter showing pre-optimized values.

Discussion:

All components were designed using an electromagnetic simulator to achieve given inductance and capacitance values at 50GHz. Of special concern were the inductors because of their poor self resonance frequencies (SRF). After the SRF, the inductance has been found to be unpredictable and leads to poor results.

Optimization Process:

- The initial starting point was found from the *ADS* simulation [ADS]. The *ADS* optimizer was given a range of practical and feasible values for the components with which to construct the filter. Since *ADS* uses the simplest lumped element

components, there is a significant difference between the results in *ADS* and from the electromagnetic simulator.

Initial Starting Point:

$C_1 = 40fF$

$L_1 = 210$ pH

$L_2 = 785$ pH

$C_2 = 7.1fF$

- A wide range of values of close to 20% of the initial starting point value were simulated in Sonnet *em*[Sonnet]. The range of simulation values were adjusted to ensure that the optimum solution was within the range of available values. The optimum solution was chosen as the solution with the lowest S_{11} at 50GHz. Simulations were also carried out to determine the coupling models. All component pairings were simulated to determine coupling models.

Simulation Range:

$48.1fF > C_1 > 32.2fF$

$216pH > L_1 > 174pH$

$866pH > L_2 > 522pH$

$28.6fF > C_2 > 6.1fF$

After all simulations were finished, 5 possibilities for each component were available.

Figure 4-25 demonstrates part of the range of data now available in optimization processes. From this graph it can be seen how the peak and bandwidth of the band pass filter change with variations to its passive components.

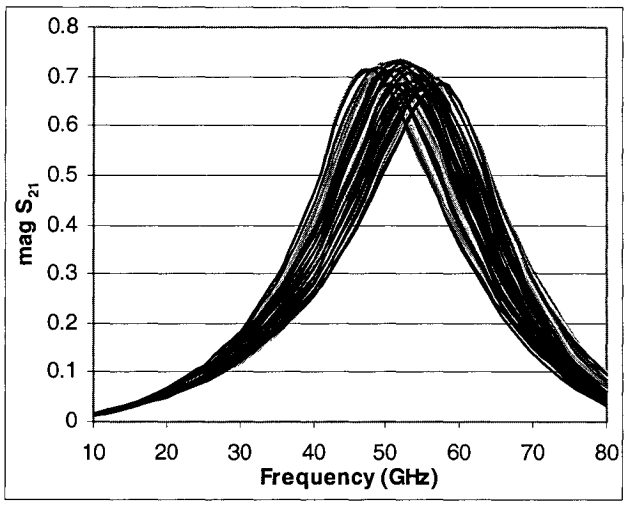

Figure 4-25. Optimization Simulations using coupling models of a 50 GHz band pass filter.

After the best available fit was found, the optimized band pass filter is compared to the original band pass filter in figure 4-26 and 4-27. The new filter yields an improvement over the un-optimized filter. Coupling models are again accurate while simulations that do not include coupling are not as accurate.

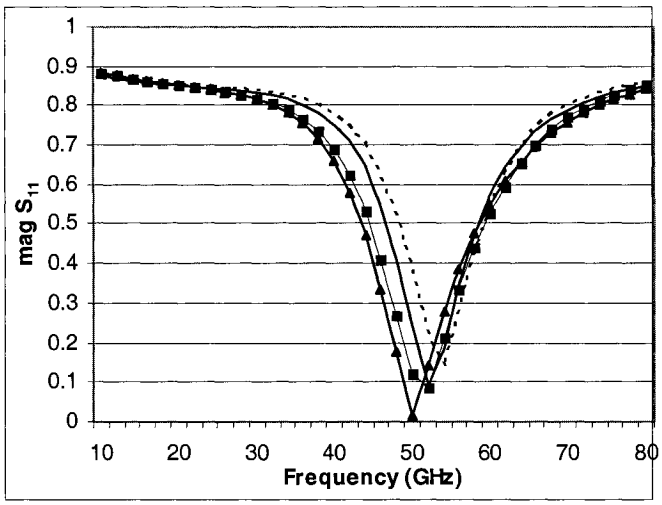

Figure 4-26. Magnitude of the S_{11} parameter of Band pass filter: Comparing the Initial band pass filter including coupling (—) and the Initial band pass filter without coupling (- -) to the Optimized band pass filter including coupling (-▲-) and the Optimized band pass filter without coupling (-■-).

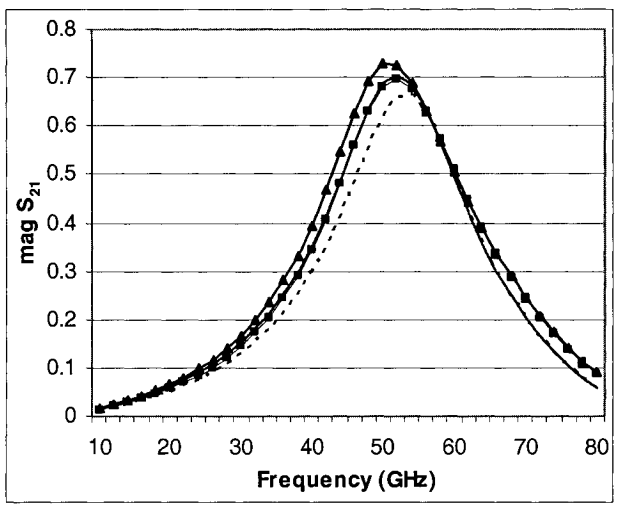

Figure 4-27. Magnitude of the S_{21} parameter of Band pass filter: Comparing the Initial band pass filter including coupling (—) and the Initial band pass filter without coupling (- -) to the Optimized band pass filter including coupling (-▲-) and the Optimized band pass filter without coupling (-■-).

As a result of the optimization process, the filter S_{21} parameter was substantially increased from the initial starting point. After the optimization was completed, a full simulation of the circuit was performed in Sonnet *em* to verify the accuracy of the coupling models as shown in figures 4-28 to 4-30. As a consequence of this research, high frequency EM optimization processes can be enabled that require large volumes of fine data. After 65GHz, there is some appreciable error that can be attributed to the limitations of using coupling models.

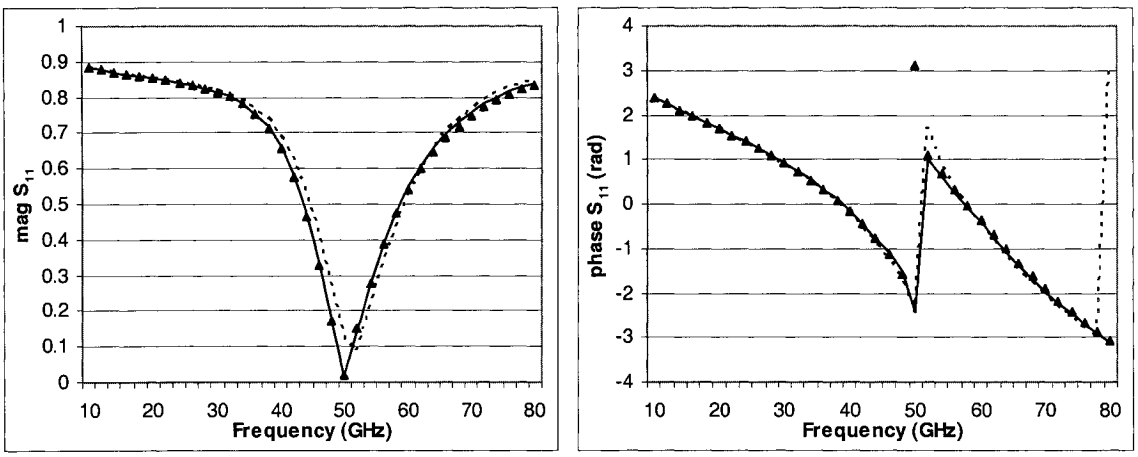

Figure 4-28. Band pass filter: Comparison of S_{11} magnitude and angle obtained by using coupling models (—) with those simulated in Sonnet (▲) and assuming no coupling (- -).

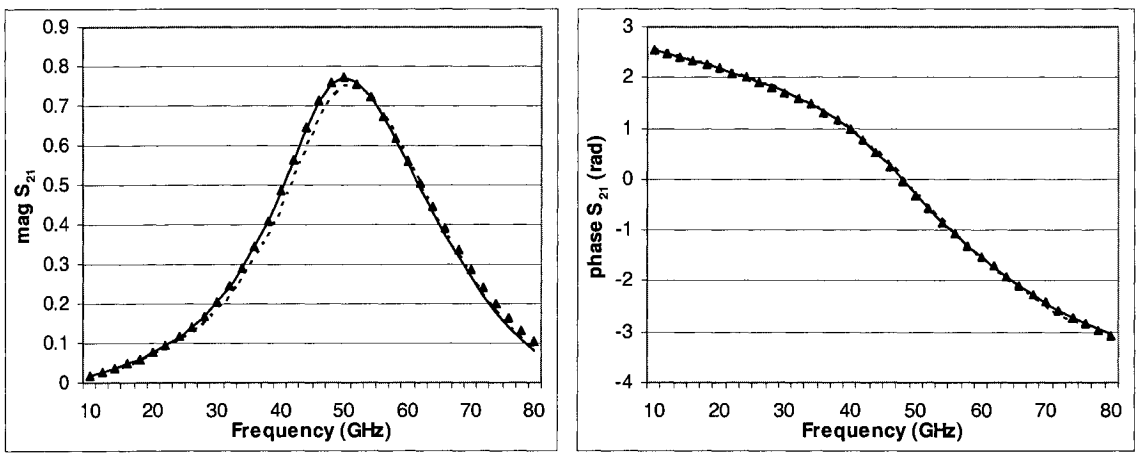

Figure 4-29. Band pass filter: Comparison of S_{21} magnitude and angle obtained by using coupling models (—) with those simulated in Sonnet (▲) and assuming no coupling (- -).

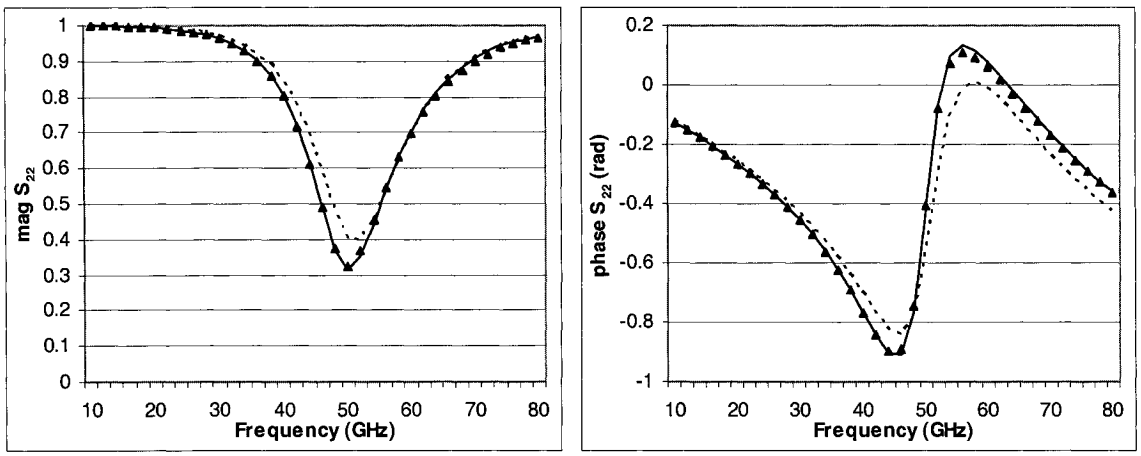

Figure 4-30. Band pass filter: Comparison of S_{22} magnitude and angle obtained by using coupling models (—) with those simulated in Sonnet (▲) and assuming no coupling (- -).

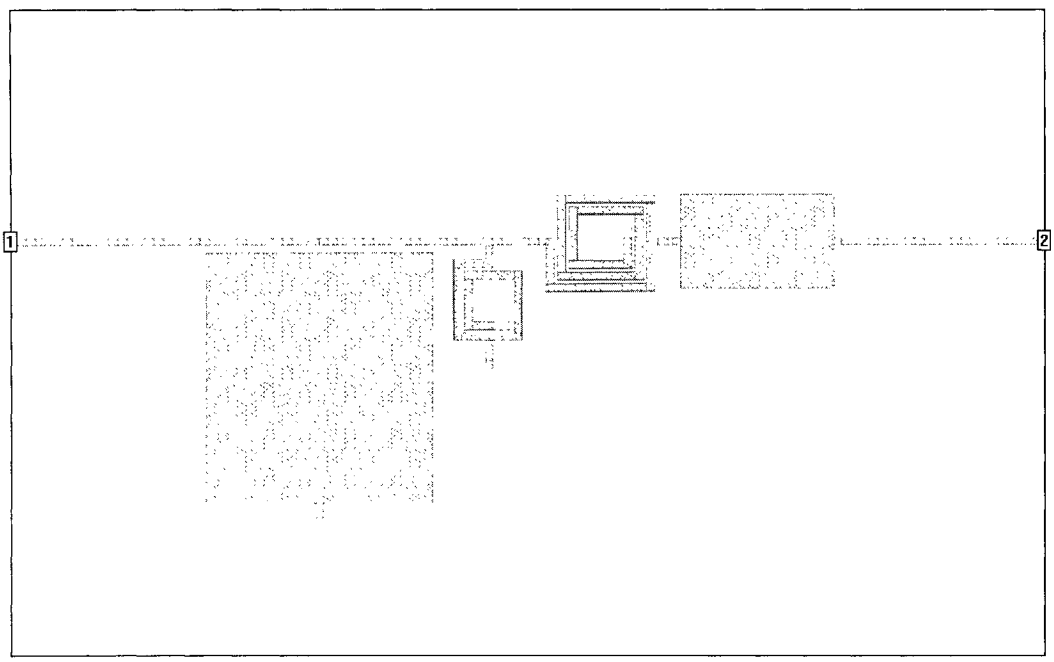

Figure 4-31. Optimized filter layout.

Table 4-2. Initial and final passive component parameters.

Passive to be Optimized	Initial Value	Final Value
C_1	44 fF	40 fF
L_1	210 pH	174 pH
L_2	785 pH	643 pH
C_2	7.1 fF	10.8 fF

The filter was laid out with optimization in mind. Every component had a single optimizable layout dimension. The capacitor plate length could be adjusted thereby adjusting the capacitance. The inductors inner and outer square length could be adjusted in order to obtain optimized inductance values. Automation was essential in this process as there were over 600 different and complex geometries to be considered.

In order to make use of integrated instead of distributed inductors, we made use of dual layer inductors. Dual layer inductors were ideal in this case since they consume less area which increases the inductor SRF.

Lastly, all models were exported into a circuit simulator, namely *ADS*. The band pass filter was implemented using S2PMDIF components as shown in figure 4-32. Examples of S2PMDIF files for both a capacitor and for a coupling model are provided in Appendix V.

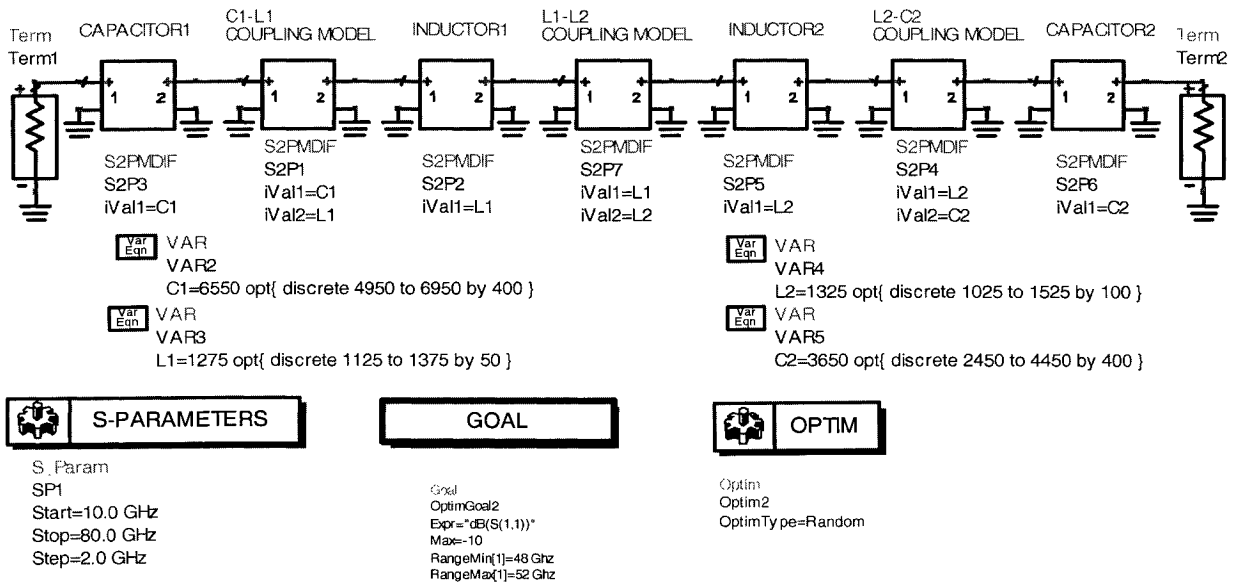

Figure 4-32. Band pass filter optimization in Agilent *ADS*.

The figure above demonstrates how a band pass filter can be optimized in *ADS* while using coupling components. As before, the circuit is optimized for smallest S_{11} at 50GHz. Each passive element can be adjusted through a single variable which corresponds to specific dimension of a passives geometry (e.g. C1 was the length of the capacitor plates in nm). The benefit of employing a circuit simulator in this application was the availability of numerous tools such as for optimization.

To demonstrate the efficiency of coupling models, it is useful to examine the time needed for setup and analysis. In this optimization 5 possibilities for each component were considered to achieve a 20% range of values. As shown in table 3.2, this would require 20 small 1-component simulations and 75 2-component simulations. The only available classical approach to perform these simulations which also includes all coupling is to simulate the

entire structure. Thus, all 625 different structures need to be simulated. This setup time is summarized below:

Proposed Approach

Initial Set-up time

20 1-component Simulations X 1800s = 10 hrs

75 2-component Simulations X 2340s = 48.75 hrs

Analysis time

45s required in *Matlab*

75s needed to run an optimize using *ADS*

Models can be reused

Compared to classical approach

625 structures X 3400s = 590.3 hrs

The setup and analysis time of the proposed approach was roughly 10 times less than by using the classical approach for this circuit configuration with both methods having the same level of accuracy. It should be stressed that models generated with the proposed approach can easily be reused for other applications, whereas each simulation for the classical approach are very specific to each circuit and cannot be easily reused.

A single structure (no optimization) can be simulated in *ADS* in slightly more than 3s while an optimization process takes close to 75s. The optimization does not necessarily yield superior results to those shown in figures 4-28 to 4-30 since the optimizer will only just meet the requirements and not necessarily exceed them. Before (figures 4-28 to 4-30), the configuration with the lowest possible S_{11} was selected.

A comparison of the previously optimized band pass filter (shown in figure 4-31 with values in Table 4-2) with a band pass filter optimized in *ADS* is demonstrated in figure 4-33. The results show that the optimized filter from *ADS* may meet the specified optimization criteria but is not the best possible configuration. Figure 4-34 compares the optimized filter to the expected results which prove the models to be accurate.

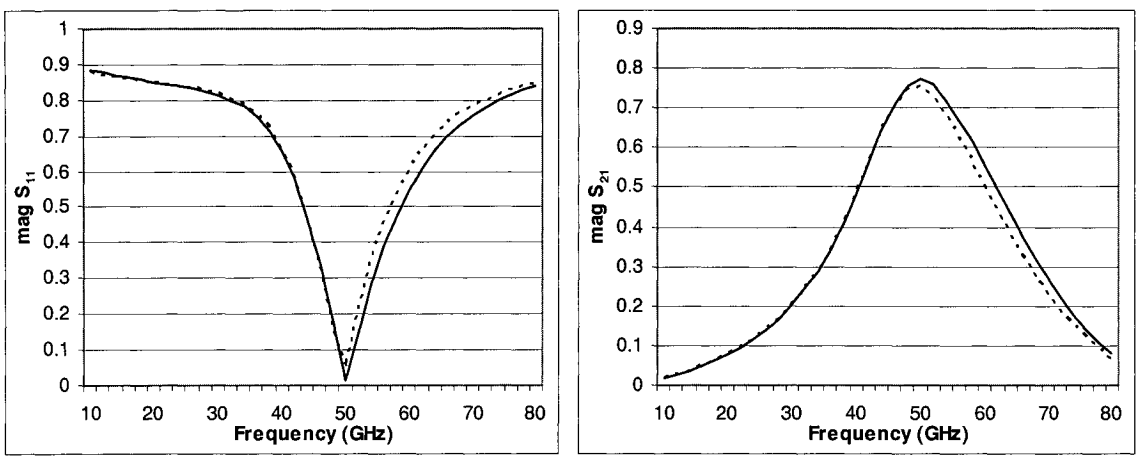

Figure 4-33. Optimized Band pass filter: Comparison of S_{11} magnitude and S_{21} magnitude obtained from a best-fit optimization process (—) to an optimization process as shown in figure 4-32(- -).

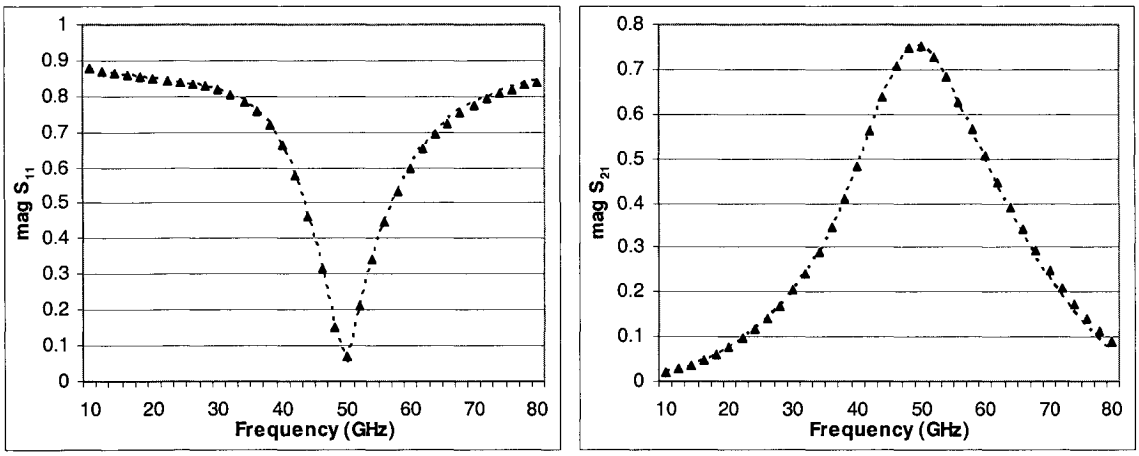

Figure 4-34. Band pass filter: Comparison of S_{11} magnitude and S_{21} magnitude obtained by using optimization process as shown in figure 4-32 (- -) with those simulated in Sonnet (▲).

4.5 Conclusion

The proposed method for obtaining methods as outlined in chapter 3 was experimentally verified in this chapter. The accuracy employing coupling models in circuit simulators was very high. Secondly, the usefulness of coupling models was highlighted in an example of optimization. It was shown that coupling models can be immensely useful in optimization problems that require full-wave EM simulations. By employing coupling models, the range and precision of data can be greatly increased at a reasonable cost in simulation time.

4.6 References

[ADS] *ADS 2004A*, Agilent Technologies, Palo Alto CA.

[Matlab] *Matlab 7*, The Mathworks Inc, Natick, MA.

[Sonnet] Sonnet 9.52, Sonnet Software Inc., Liverpool, NY.

CHAPTER V

CONCLUSIONS AND FUTURE WORK

5.1 Conclusion

Based on future requirements for advanced circuit design and optimization, the use of lumped elements is on the verge of finding application in millimetre wave designs. As such, development of new techniques and tools for passive design is essential. It was shown in this thesis that coupling can have a major effect at these frequencies and then, has to be efficiently computed. However, currently there exists no method for accurately and quickly modeling the coupling effect for use in circuit design.

Thus, an efficient approach for modeling of parasitic coupling has been presented. Applied to various microwave integrated circuits, the proposed technique demonstrated its efficiency in terms of speediness and ease of usage. It helps making the design of microwave integrated circuits faster, more accurate and efficient, contributing to overall reductions in design cycles. The library of neural network models and the N-ports T-

parameters internal codes can be subsequently used for the simulation and optimization of more complex microwave circuits.

While considering an optimization of a band pass filter, it was found that coupling models can be used to quickly and accurately represent 625 different filter configurations. The simulation of every model took just 45s in Matlab and was shown to be as accurate as in a full wave circuit simulator. Finally, an optimization process was also performed using coupling models in a circuit simulator. Bringing coupling models forward into circuit design space was very important for enhancing the speed of simulation as well as making available the wealth of tools associated with a circuit simulator.

5.2 Future Work

This thesis represents the first time coupling has been modeled for passive circuit design. There are many areas where this topic needs to be further developed before it can gain general acceptance.

- First, stronger examples using coupling models in larger circuits need to be implemented. How accurate are the results of using coupling models with a very large circuit of more than 20 components? How close can non-adjacent components be before the error becomes too large? Questions such as these need to be investigated.

- Yield optimization is an exciting area of research using coupling models. Coupling models are uniquely suited to this application since they are well suited to generating large ranges of data.

- Circuit modification is a major application of coupling models. If a library of components with associated coupling models is available, then modification to passive circuits can be performed almost instantly, as opposed to waiting for new full wave simulations. Due to its potential for time savings, this is an exciting area of research.

- Given a generic circuit layout, automatic microwave passive circuit generation using coupling models is possible. To generate the coupling model for a single component, only a small piece of the overall circuit would need to be re-simulated. Thus an automated tool could choose which piece of the circuit should be altered, automatically drive the full wave simulator and insert the new model back into the circuit simulator. Coupling models are essential for this process. Using conventional approaches, components could be accurately modeled, but the entire circuit simulation would not be accurate since mutual coupling would not be present. By employing full wave models of passive components as well as coupling models, it is possible to use circuit simulators to optimize designs.

- While discrete optimization has been demonstrated in this thesis, it is possible that Neural Networks can be used to model coupling components to generate a continuous

optimization process. Thus, optimized component parameters down to smallest scalable geometry can then be implemented, instead of down to the next discrete value.

- Coupling between active and passive components needs to be modeled to enable the modeling of complete circuits. There has been some work done in this field but it is not yet mature. This important research would enable the optimization of an entire functioning design with active and passive components.

APPENDIX I

Solving S-parameter Equations for a 3-port component in terms of its internal components

By using the connection scattering matrix representation for a 3 port circuit, the overall 3-port S-parameter matrix is solved. Figure A1-1 is an example 3-port circuit which has 4 internal components represented by S-paramters S_A, S_B, S_C and S_X. In Appendix II, the 9 equations for the overall S-parameters are used to solve for the 9 unknowns in S_X.

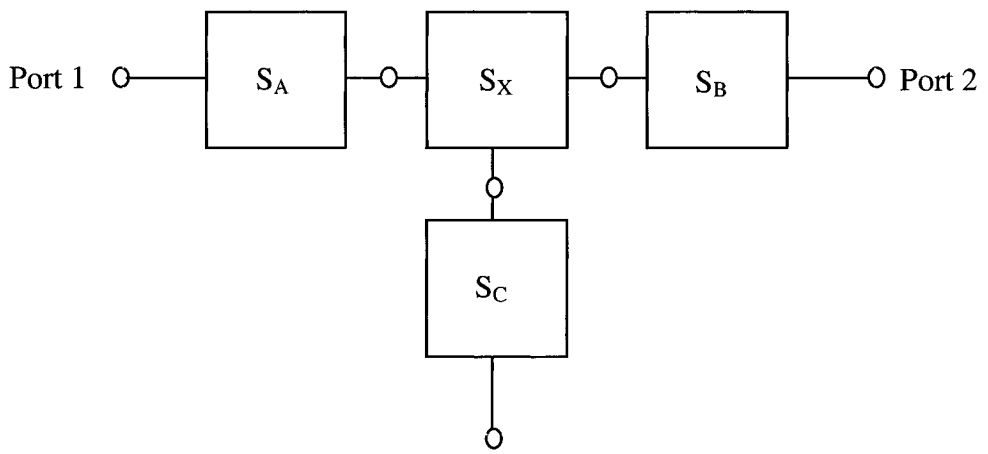

Figure A1-1. Example 3-port circuit used to derive equations for overall 3-port S-parameters.

S11t = (TT1+TT2 +TT3 +TT5)/Den1
S21t = TT6/Den1
S31t = TT7 /Den1
S12t = TT8 /Den1
S22t = (TT9+TT10+TT11+TT12+TT13) /Den1
S32t = (TT14) /Den1
S13t = (TT15) /Den1
S23t = (TT16) /Den1
S33t = -(TT17+TT18+TT19+TT20+TT21) /Den1

where
Den1 = (TT22+TT23)

T1 = S11a S22a
T2 = S12a S21a
T3 = S11b S11c
T4 = T21 S11c
T5 = S11x T13
T6 = S13x S22x S31x
T7 = S23x S32x
T8 = S11x S33x
T9 = T11 S33x
T10 = S13x S21x S32x
T11 = S12x S21x
T12 = S13x S31x
T13 = S22x S33x
T14 = S12x S23x S31x
T15 = S21a S21b
T16 = S11x S22x
T17 = S11a S11b
T18 = S11c S33x
T19 = T22 S11c
T20 = S22a S22b
T21 = S11b S22b
T22 = S12b S21b
T23 = S21a S21c
T24 = S12a S12b
T25 = S12b S21c
T26 = S12a S12c
T27 = S21b S12c
T28 = S12c S21c
T29 = S22a S22c
T30 = S11c S22c
T31 = S22a S11b

TT1 = S11x (T1-T2+T2 T3 T7-T1 T3 T7)
TT2 = S11a (T18-1+T3 T7 -T3 T13)
TT3 = S11c (T2 T8 -T2 T12-T1 T8 +T1 T12)
TT4 = S11b (T2 T16-T2 T11 +T1 T11)
TT5 = T17 S22x-T17 S22a T16 +T2 T3 T6 -T2 T3 T5 +T1 T3 T5 -T2 T3 T14 +T1 T3 T14 -T1 T3 T6+T1 T3 T10 -T2 T3 T10+T2 T3 T9-T1 T3 T9
TT6 = T15 (-S21x+S11c S21x S33x-S11c S23x S31x)
TT7 = T23 (-S11b S21x S32x-S31x+S11b S22x S31x)
TT8 = T24 (-S11c S13x S32x-S12x+S11c S12x S33x)
TT9 = S22a (-T19 T14-T19 T5 -T4 S11x T7+T19 S11x T7 +T19 T6+T4 T5 -T4 T6+T4 T14+T4 T10+T19 T9-T19 T10-T4 T9+T22 T16 -T21 T16-T22 T11+T21 T11)
TT10 = S22b (T18-1)
TT11 = S11c (T20 T12 -T20 T8)
TT12 = S22x (-T22 +T21)

TT13 = T4 T7-T19 T7 +T19 T13 -T4 T13 +T20 S11x
TT14 = T25 (-S22a S12x S31x-S32x+S22a S11x S32x)
TT15 = T26 (S11b S13x S22x-S11b S12x S23x-S13x)
TT16 = T27 (-S22a S13x S21x-S23x+S22a S11x S23x)
TT17 = S11b (-S22c S22x-T29 S11c T10-T29 T11+T29 T16+T28 T7-T28 T13)
TT18 = S22a (-T28 T8+T28 T12)
TT19 = S22c (1-T3 T7+T3 T13)
TT20 = S11x (-T29+T29 T3 T7-T31 T28 T7)
TT21 = -T30 S33x+ T28 S33x +T31 T28 T10+T29 T3 T9-T31 T28 T9 +T31 T28 T14 - T31 T28 T6+T31 T28 T5 -T29 T3 T14+T29 T3 T6-T29 S11c T12-T29 T3 T5 +T29 S11c T8
TT22 = S22a (T3 T10-T3 T9-S11c T8-T3 S11x T7+S11c T12-T3 T6+T3 T5+S11x+T3 T14)
TT23 = T31 T11+T3 T7 -1 -T31 T16+S11b S22x+T18 -T3 T13

APPENDIX II

S-Parameter Equations to model Coupling In a 3-port component

Equations for S_X:

S11x = (TT24 + TT25 + TT26 + TT27 + TT28 + TT29)/Den2
S21x = TT30/Den2
S31x = TT31/Den2
S12x = -S12a/Den2
S22x = (TT32 + TT33 + TT34 + TT35 + TT36)/Den2
S32x = (TT37)/Den2
S13x = (TT38)/Den2
S23x = (TT39)/Den2
S33x = (TT40+TT41+TT42+TT43)/Den2

Where
Den2 = TT44+TT45+TT46+TT47+TT48

T32 = S13t S31t
T33 = S12t S21t
T34 = S23t S32t
T35 = S11c S11t
T36 = T40 S33t
T37 = S13t S22t S31t
T38 = S13t S21t S32t
T39 = S22t S33t
T40 = S11t S22t
T41 = S12t S23t S31t
T42 = S11t S33t
T43 = S11b S22c S22t
T44 = S11c S33t
T45 = S22a S11c

TT24 = S11c (-T22 T32+ T32 T21)
TT25 = +S11b (T33 T30-T28 S12t S21t-T30 T40+ T28 T40)
TT26 = S11a (-T25 T27- T22 S11c S33t+ T3 T34- T3 T39+ T30 T22
TT27 = S22b (-T30 T17+ T44 T17+ T28 T17)
TT28 = S11t (-T22 T30 +T25 T27-T3 T34-T28 T21+T30 T21)
TT29 = T3 S13t S21t S32t-T3 T33 S33t- T3 T37 +T3 S12t S23t S31t +T30 T17 S22t
+T3 T36 - T17 T28 S22t +T22 T35 S33t -T35 S33t T21
TT30 = T15 (-T30 S12t +S11c S12t S33t-S11c S13t S32t+ T28 S12t)
TT31 = T23 (S11b S13t S22t-S11b S12t S23t+T22 S13t -S13t T21)

TT32 = S22a (-T44 T33+ T28 T40- T28 T33+ T35 T39-T30 T40+ T30 T33- T35 T34)
TT33 = S11c (T20 T32+ T1 T34- T1 T39 +T2 T39- T2 T34)
TT34 = S22b (-T2 T28 -T2 T44 -T30 T1 + T1 T44+T2 T30+ T1 T28)
TT35 = S22t (T2 T28 +T30 T1 - T1 T28 - T2 T30)
TT36 = T45 S12t S23t S31t- T45 T37 + T45 T38 +T30 T20 S11t - T28 S11t T20- T35 S33t T20
TT37 = -T1 T25 S23t+ S22a T25 S11t S23t+ T25 S23t T2 - S22a T25 S13t S21t
TT38 = -S12a S11b S12c S21t S32t -T26 S31t T22 -S12a S11b S12c S22t S31t-T26 S31t T21
TT39 = (S22a S11t S32t - S22a S12t S31t +S32t T2- T1 S32t) T27
TT40 = S33t (-T1 T22 + T24 T15-T2 T21+ T20 T17- T31 T33)
TT41 = S22a (T22 T42 - T22 T32 + T32 T21 - T42 T21) + S22c (T1 T22 - T24 T15 - T20 T17- T31 T40 +T2 T21) - S22a T22 S22c S11t
TT42 = S11b (T2 T39 - T1 T39 + T1 T34 + T33 T29 - T34 T2)
TT43 = -T31 T37 + T31 T41 + T1 T43 + T31 T36 -T2 T43+ T31 T38 + T29 S11t T21 - T31 S11t T34

TT44 = S22a (-T22 T30 S11t- T22 S11c T32+ T3 T41+T25 T27 S11t+ T22 S11c T42- T3 T37+ T3 T36 + T3 T38+T30 T21 S11t- T28 S11t T21- T35 S33t T21- T3 S11t S32t S23t- T3 T33 S33t)
TT45 = S11b S22t (T2 T28 + T30 T1- T1 T28)
TT46 = T44 (T24 T15- T1 T22 - T2 T21+ T20 T17)
TT47 = T30 (T1 T22 - T24 T15+T2 T21- T31 T40+ T31 T33- T20 T17)
TT48 = -T25 T1 T27 + T24 T28 T15- T31 T28 T33 + T45 T32 T21 - T2 T28 T21 + T31 T28 T40 +T2 T3 T39 - T1 T3 T39 + T1 T3 T34 -T2 T3 S22c S22t + T20 T28 T17 -T3 T34 T2

APPENDIX III

Lowpass Chebyshev design equations

In a Chebyshev filter, the attenuation loss is expressed in the following equation:

$$A_m = 10\log[1+(10^{Am/10}-1)\cos^2(n\cos^{-1}\omega')] \qquad \text{(A3.1)}$$

Using the above formula, it was determined that a 7th order filter was required. Next the g_k values are calculated as follows:

$$g_o = 1$$

$$g_1 = \frac{2a_1}{\gamma}$$

$$g_k = \frac{4a_{k-1}a_k}{b_{k-1}g_{k-1}} \qquad k = 2,3,...n$$

$$g_{n+1} = 1 \qquad n \text{ odd}$$

$$g_{n+1} = \coth^2(\beta/4) \qquad n \text{ even}$$

$$a_k = \frac{\sin(2k-1)\pi}{2n} \qquad k = 1,2...n$$

$$b_k = \gamma^2 + \sin^2(\frac{k\pi}{n}) \qquad k = 1,2...n$$

$$\beta = \ln(\coth\frac{Am}{17.37})$$

$$\gamma = \sinh(\frac{\beta}{2n}) \qquad \text{(A3.2)}$$

Given all g_k values, the lowpass filter can be realized using series inductors and shunt capacitors.

$$L_k = g_k\frac{Z_o}{\omega_{LP}}$$

$$C_k = g_k\frac{1}{\omega_{LP}Z_o} \qquad \text{(A3.3)}$$

where Zo is the load impedance and w_{LP} is the cutoff frequency.

APPENDIX IV

INDUCTORS AND SELF RESONANT FREQUENCIES

Inductors are a special concern in design since inductor self resonance frequencies (SRF) can occur at frequencies as low as 6GHz. Inductor SRF is the frequency where the inductor Quality factor (Q) reaches 0. Recent research has shown that the inductor SRF can be increased by choosing smaller layout area[Dick04] [Dick05] to avoid substrate loss[Liou]. Several modifications to layout were performed in order to increase the inductor SRF well beyond 50 GHz. These modifications included decreasing the inductor area by selecting smaller line width and line spacing as well as utilizing a 2-level stacked structure[Dick04].

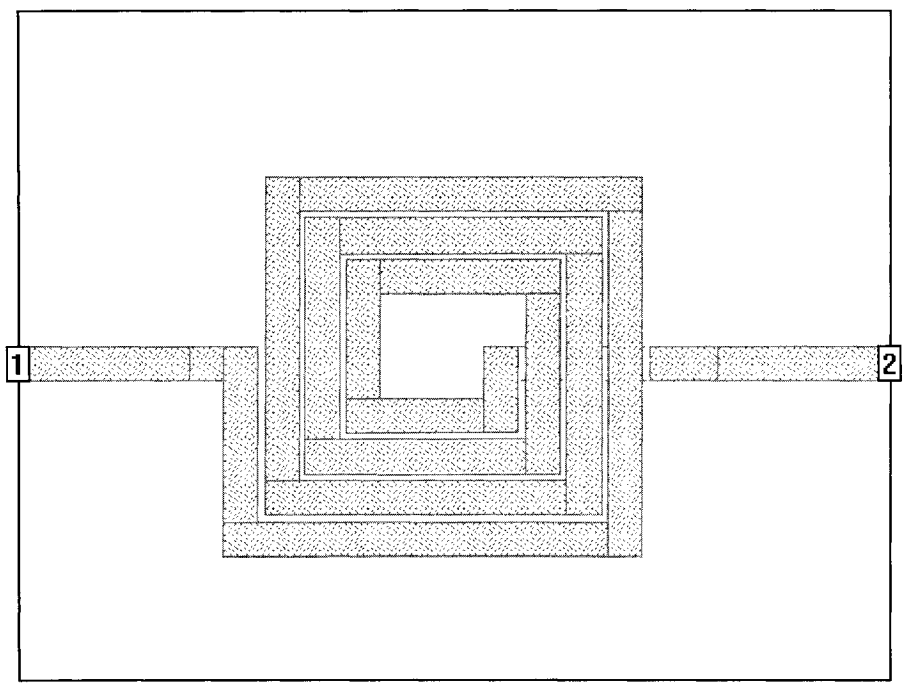

Figure A4-1. Inductor A: Single layer Inductor. Exhibits 1.16 nH at 10GHz. 3.5 turns, line width = 10μm, line spacing = 2μm. Layout area = 121μm X 110μm.

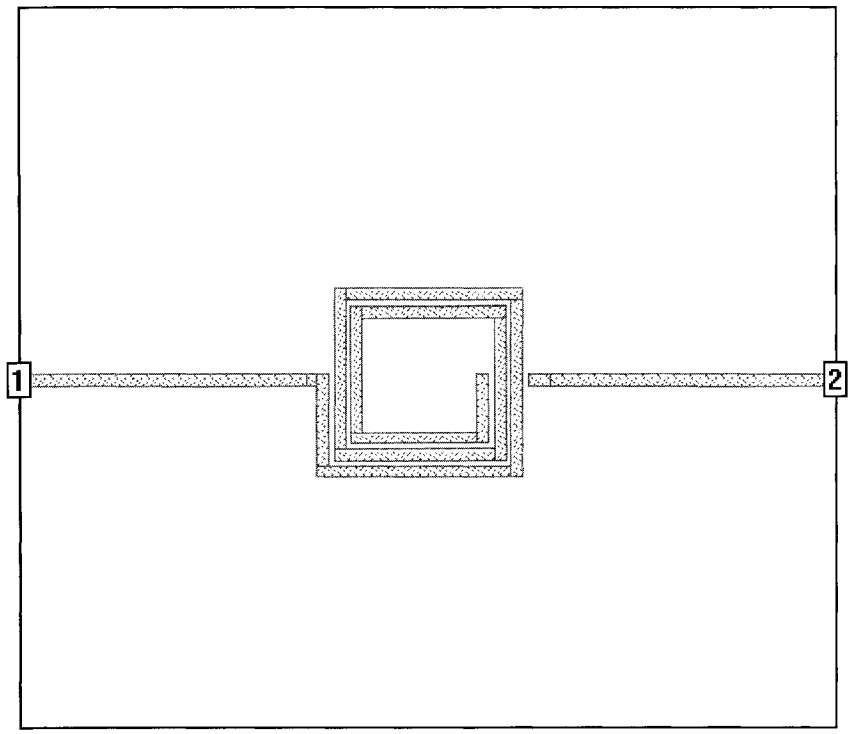

Figure A4-2. Inductor B: Double layer inductor. Exhibits 0.98 nH at 10GHz. 2.5 turns top and 2 turns bottom. Line width = 2μm, line spacing = 1μm, inside square length = 20μm.

Inductor A is a single layer inductor which implies that the inductors turns are only on the top layer. A double layer inductor is shown in fig. A4-3 which has turns on two layers.

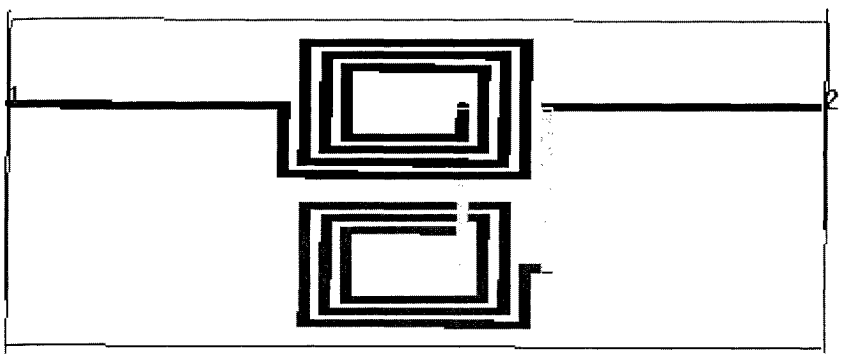

Figure A4-3. 3 Dimensional View of a Double Layer inductor.

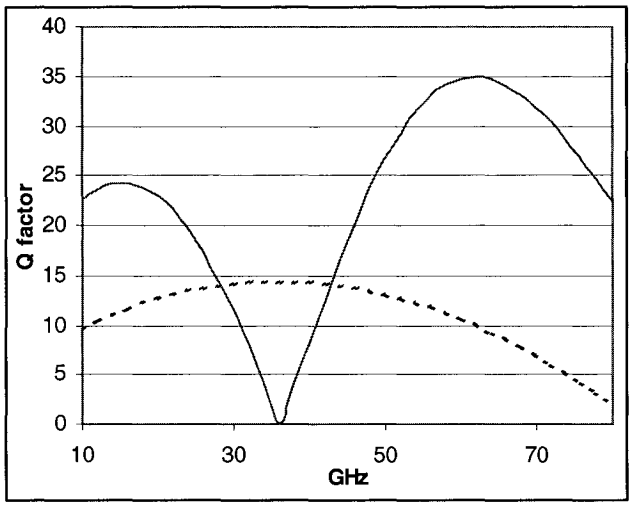

Figure A4-4. Q-factor comparison of a Single Layer Inductor (—) and a Double Layer Inductor (----).

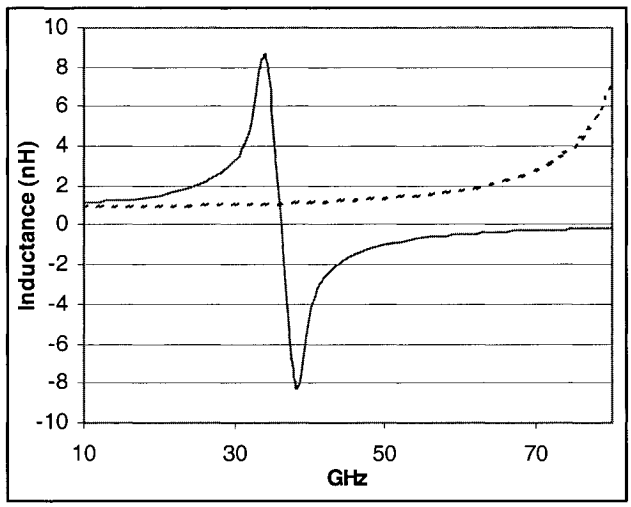

Figure A4-5. Inductance comparison of a Single Layer Inductor (—) and a Double Layer Inductor (----).

The results agree with previous research. Inductor B has higher SRF than inductor A since inductor B consumes less area. Many other methods have been presented to increase SRF such as patterned ground shields [Burg98] to reduce substrate resistance and tapered trace width but are not investigated here.

Appendix IV References

[Dick04] T. Dickson, M. Lacroix, S. Boret, D. Gloria, R. Beerkens, S. Voinigescu, "Si-based Inductors and Transformers for 30-100GHz applications," *IEEE MTT-S Int. Microwave Symp. Dig.*, 2004, 205-208.

[Dick05] T. Dickson, M. Lacroix, S. Boret, D. Gloria, R. Beerkens, S. Voinigescu, "30-100 GHz Inductors and Transformers for Millimeter-Wave (Bi)CMOS Integrated Circuits," *IEEE Trans. On Microwave Theory and Tech.*, 2005, 123-133.

[Liou] J.J. Liou, "On-Chip Spiral Inductors for RF Applications," Application Note, University of Central Florida.

[Burg98] J.Burghartz, "Progress in RF Inductors on Silicon – Understanding Substrate Losses," *IEDM '98 Technical Digest.*, 1998, 523 – 526.

APPENDIX V

Sample S2PMDIF Files

First for two discrete capacitors:

```
VAR      C1       =          4950
BEGIN    ACDATA
#        hz       s          ma       r          50
  1E+10  0.008661 -22.8726   0.991626 -5.37903   0.991626 -5.37903   0.008661 -22.8726
1.2E+10  0.009938 -31.3637   0.99081  -6.41537   0.99081  -6.41537   0.009938 -31.3637
  ...    ...      ...        ...      ...       ...       ...       ...      ...
7.8E+10  0.365681 -149.628   0.872091 -57.512    0.872091 -57.512    0.365681 -149.628
  8E+10  0.403559 -153.564   0.849286 -60.8038   0.849286 -60.8038   0.403559 -153.564
END      ACDATA

VAR      C1       =          5350
BEGIN    ACDATA
#        hz       s          ma       r          50
  1E+10  0.010345 -42.6076   0.991595 -5.58312   0.991595 -5.58312   0.010345 -42.6076
1.2E+10  0.012433 -50.2498   0.990761 -6.66228   0.990761 -6.66228   0.012433 -50.2498
  ...    ...      ...        ...      ...       ...       ...       ...      ...
7.8E+10   0.45483 -156.493    0.8184  -63.3317    0.8184  -63.3317    0.45483 -156.493
  8E+10  0.499323 -161.078   0.784094 -67.2028   0.784094 -67.2028   0.499323 -161.078
END      ACDATA
```

Second for a coupling component between a capacitor and an inductor. Only the inductor is swept here.

```
VAR      C1       =          4950
VAR      L1       =          1125
BEGIN    ACDATA
#        ghz      s          ma       r          50
     10  0.004768 -93.576    1.0017  -0.26849    1.0017  -0.26849    0.005263 -45.993
     12  0.002839 -110.86    1.0011  -0.15416    1.0011  -0.15416    0.003598 -28.713
...      ...      ...        ...      ...       ...       ...       ...      ...
     78  0.044365  121.01    0.99764   2.2135   0.99764   2.2135    0.04225   66.999
     80  0.048145  121.52    0.99755   2.4136   0.99755   2.4136    0.045748  66.414
```

```
END     ACDATA

VAR     C1      =       4950
VAR     L1      =       1175
BEGIN   ACDATA
#       ghz     s       ma      r               50
      10 0.004186  -95.921  1.0015   -0.234  1.0015   -0.234  0.004664  -43.573
                                             -        -
      12 0.002428  -116.88  1.0009  0.12551  1.0009  0.12551  0.003185  -23.395
   ...    ...     ...     ...     ...     ...     ...     ...     ...
      78 0.043232  121.29  0.99769  2.1637  0.99769  2.1637  0.041133  66.717
      80 0.046879  121.83  0.9976   2.357   0.9976   2.357   0.044502  66.11
END     ACDATA
```